

This discussion paper is/has been under review for the journal Atmospheric Chemistry and Physics (ACP). Please refer to the corresponding final paper in ACP if available.

**Ozone response to  
emission changes**

J. Song et al.

# Ozone response to emission changes: a modeling study during the MCMA-2006/MILAGRO campaign

**J. Song<sup>1,2</sup>, W. Lei<sup>1,2</sup>, N. Bei<sup>1</sup>, M. Zavala<sup>1</sup>, B. de Foy<sup>3</sup>, R. Volkamer<sup>2,4</sup>,  
B. Cardenas<sup>5</sup>, J. Zheng<sup>6</sup>, R. Zhang<sup>6</sup>, and L. T. Molina<sup>1,2</sup>**

<sup>1</sup>Molina Center for Energy and the Environment, CA, USA

<sup>2</sup>Department of Earth, Atmospheric and Planetary Sciences, Massachusetts Institute of Technology, MA, USA

<sup>3</sup>Department of Earth and Atmospheric Sciences, Saint Louis University, USA

<sup>4</sup>Department of Chemistry and Biochemistry, University of Colorado at Boulder, CO, USA

<sup>5</sup>National Institute of Ecology (INE), Mexico

<sup>6</sup>Department of Atmospheric Sciences, Texas A&M University, TX, USA

Received: 20 October 2009 – Accepted: 22 October 2009 – Published: 3 November 2009

Correspondence to: W. Lei (wlei@mit.edu)

Published by Copernicus Publications on behalf of the European Geosciences Union.

Title Page

Abstract

Introduction

Conclusions

References

Tables

Figures

◀

▶

◀

▶

Back

Close

Full Screen / Esc

Printer-friendly Version

Interactive Discussion



## Abstract

The sensitivity of ozone production to precursor emissions was investigated under five different meteorological conditions in the Mexico City Metropolitan Area (MCMA) during the MCMA-2006/MILAGRO field campaign using the gridded photochemical model CAMx driven by observation-nudged WRF meteorology. Precursor emissions were constrained by the comprehensive data from the field campaign and the routine ambient air quality monitoring network. Simulated plume mixing and transport were examined by comparing with measurements from the G-1 aircraft during the campaign. The observed concentrations of ozone precursors and ozone were well reproduced by the model. The effects of reducing precursor emissions on urban ozone production were performed for three representative emission control strategies. A 50% reduction in VOC emissions led to 7 to 22 ppb decrease in daily maximum ozone concentrations, while a 50% reduction in NO<sub>x</sub> emissions leads to 4 to 21 ppb increase, and 50% reductions in both NO<sub>x</sub> and VOC emission decrease the daily maximum ozone concentrations up to 10 ppb. These results along with a chemical indicator analysis using the chemical production ratios of H<sub>2</sub>O<sub>2</sub> to HNO<sub>3</sub> demonstrate that the MCMA urban core region is VOC-limited for all meteorological episodes, which is consistent with the results from MCMA-2003 field campaign; however the degree of the VOC-sensitivity is higher in the MCMA-2006 due to lower VOC/NO<sub>x</sub> emission ratio and VOC reactivity. Ozone formation in the surrounding mountain/rural area is mostly NO<sub>x</sub>-limited, but can be VOC-limited, and the range of the NO<sub>x</sub>-limited or VOC-limited areas depends on meteorology.

## 1 Introduction

The Mexico City Metropolitan Area (MCMA), shown in Fig. 1, is located in the Valley of Mexico. With nearly 20 million inhabitants, Mexico City is North America's most populous city and one of the largest megacities in the world. As a result of rapid increase

## Ozone response to emission changes

J. Song et al.

Title Page

Abstract

Introduction

Conclusions

References

Tables

Figures

◀

▶

◀

▶

Back

Close

Full Screen / Esc

Printer-friendly Version

Interactive Discussion



in population and urbanization, Mexico City suffers from serious air pollution problems (Molina and Molina, 2002; Molina and Molina, 2004). The urban emissions also significantly influence air quality on the regional scale (Mena-Carrasco et al., 2009).

Ozone photochemical production is high in Mexico City due to high emissions of NO<sub>x</sub> and VOCs, which provide elevated radical sources, the driving force for urban photochemical activity (Volkamer et al., 2007; Sheehy et al., 2008). Both measurements and chemical transport model simulations during the MCMA-2003 field measurement campaign (Molina et al., 2007) suggest that O<sub>3</sub> production in the source region is VOC limited during the photochemically active periods (Lei et al., 2007) and weakly dependent on meteorological conditions (Lei et al., 2008). Other recent studies (Tie et al., 2007; Torres-Jardon, 2004) also suggest that O<sub>3</sub> production in the MCMA is VOC-limited, in contrast to results of earlier modeling studies (West et al., 2004; Sillman and West, 2009).

Analysis of the historical trends of O<sub>3</sub>, CO and NO<sub>x</sub> from the data collected at the air quality monitoring network Red Automática de Monitoreo Atmosférico (RAMA) suggests that ozone formation in Mexico City has moved from less VOC-limited to more VOC-limited regime (Stephens et al., 2008; Zavala et al., 2008). However, as noted in the study by Lei et al. (2007, 2008) and other results from the MCMA-2003 field campaign, VOC measurements were limited to a few sites for a relatively short period of time, which may lead to less precise interpretations of the model results.

Another major international field study, MILAGRO (Megacity Initiative: Local and Global Research Observations), was conducted in the MCMA three years later in March, 2006 to evaluate the local, regional and global impacts of the Mexico City air pollution plume (Molina et al., 2008, 2009). The measurements included a wide range of instruments at ground sites and on aircraft and satellites, which provided unprecedented comprehensive data sets over a wide geographical coverage. MCMA-2006, one of the four MILAGRO components, focused on the emissions within the Mexico City basin and their transport and transformation in the basin using extensive measurements at the T0 supersite, at multiple temporary sites and around the urban area

**Ozone response to emission changes**

J. Song et al.

[Title Page](#)[Abstract](#)[Introduction](#)[Conclusions](#)[References](#)[Tables](#)[Figures](#)[◀](#)[▶](#)[◀](#)[▶](#)[Back](#)[Close](#)[Full Screen / Esc](#)[Printer-friendly Version](#)[Interactive Discussion](#)

from mobile laboratories.

Urban and regional-scale photochemical models are typically evaluated using ground measurements, and they are rarely evaluated using arrays of aircraft measurements due to their scarcity. The evaluation of 3-D models using aircraft measurements has the potential to provide further insights to model's capabilities for capturing various processes such as vertical mixing and transport. In addition, the aircraft data also provide a unique opportunity to evaluate the interaction between emission, meteorology and chemistry near and further from the urban center.

Using a 3-D photochemical model, the Comprehensive Air quality Model with extensions version 4.40 (CAMx v4.40), this paper extends the study of Lei et al. (2007, 2008) to the MCMA-2006 field campaign. The updated version of CAMx is run over a larger domain and is driven by observation-nudged WRF meteorology. The large number of monitoring sites and measurement platforms available during MCMA-2006 are used to address two major issues: 1) the evaluation of the model performance on simulating ozone precursors and ozone; and 2) the sensitivity analysis of ozone production to the precursor emissions under different meteorological conditions using the Brute-Force method in conjunction with chemical indicator analysis. These results are compared with the corresponding findings of Lei et al. (2007, 2008) from the MCMA-2003 field campaign. The methodology for this study is introduced in Sect. 2. Simulated ozone and ozone precursors are evaluated and sensitivity studies are presented and discussed in Sect. 3, followed by comparisons with findings from the previous field campaign.

**Ozone response to emission changes**

J. Song et al.

Title Page

Abstract

Introduction

Conclusions

References

Tables

Figures

◀

▶

◀

▶

Back

Close

Full Screen / Esc

Printer-friendly Version

Interactive Discussion



## 2 Methodology

### 2.1 Measurements

#### 2.1.1 Ground-based measurements

The RAMA air quality monitoring network in the MCMA collected surface criteria pollutant concentrations and meteorological parameters at hourly intervals (<http://www.sma.df.gob.mx/simat/>). A total of 15 monitoring stations, 3 monitoring stations from each city sector (NE, NW, SE, SW, and CT), were selected based on the location representativeness and data availability of CO, NO<sub>x</sub>, and O<sub>3</sub> during the campaign period. Measurements of NO<sub>x</sub> from RAMA using the chemiluminescence technique more accurately represent gaseous NO<sub>y</sub>.

In this study, volatile organic compounds (VOCs) data reported during the MILAGRO Campaign were used to evaluate the VOC emissions in the MCMA, particularly in the urban area. VOCs were measured at T0, T1, SIMAT and CENICA. Figure 1 shows the location of these sites. At T0, the urban supersite located just north of downtown Mexico City, aldehydes and aromatics were measured with Proton Transfer Reaction Mass Spectrometry (PTR-MS) (Zhao and Zhang, 2004; Fortner et al., 2009), formaldehyde and aromatics were measured with long-path Differential Optical Absorption Spectroscopy (DOAS); another set of formaldehyde and ethene were acquired by Tunable Diode Laser Absorption Spectroscopy (TDLAS) onboard the Aerodyne mobile lab while parked at T0; and canister samples of ethene, alkanes, and aromatics were analyzed by Gas Chromatography (GC) and GC/MS. At the CENICA site, located in an urban commercial/residential area with fewer industries than T0, alkanes and aromatics from canisters were speciated by GC analysis using Flame Ionization Detection (GC-FID). At the SIMAT site (19°24' N, 99°10' W), close to the center of the city, VOC concentrations and fluxes were measured using eddy covariance (EC) techniques coupled with Fast Olefin Sensor (FOS) (Velasco et al., 2009). Measurements at the T1 site (de Gouw et al., 2008) located in the northeast urban outskirt and other sites outside

## Ozone response to emission changes

J. Song et al.

Title Page

Abstract

Introduction

Conclusions

References

Tables

Figures

◀

▶

◀

▶

Back

Close

Full Screen / Esc

Printer-friendly Version

Interactive Discussion



the MCMA were not included as they are downwind sites, containing less information about urban emissions. Table 1 lists the VOCs used in this study with their corresponding measurement techniques and operation institutions during the MCMA-2006 field campaign. A detailed summary of the ground-based and aircraft measurements of VOCs can be found in Apel et al. (2009).

### 2.1.2 G-1 aircraft measurements

During MILAGRO-2006 several aircraft were deployed in and around the MCMA to collect chemical and meteorological data, including the G-1 operated by DOE (<ftp://ftp.asd.bnl.gov/pub/ASP%20Field%20Programs/2006MAXMex/>) and the C-130 operated by NCAR (<http://mirage-mex.acd.ucar.edu/Measurements/C130/index.shtml>). In this study only measurements from G-1 were included, since the flights covered a smaller spatial and temporal domain, which is the scope of this study. There were 15 G-1 flights measuring chemical species over the MCMA, especially above T0 and T1 supersites. Details on the G-1 aircraft flights over Mexico City during MILAGRO are provided in Kleinman et al. (2008) and Nunnermacker et al. (2008). Data used in this study are 10-second average values for CO and O<sub>3</sub> on 7 March, and CO, O<sub>3</sub> and speciated VOCs on 27 March. CO and O<sub>3</sub> were measured using VUV fluorescence analyzer and UV absorption detector, respectively (Springston et al., 2005). Canister samples of ethene, alkanes and aromatics were collected every 1–2 min, and analyzed by GC. Ten-second averaged aromatics were also measured with PTR-MS.

## 2.2 Model description

Concentrations of air pollutants were simulated using CAMx v4.40 (Environ, 2006) with the SAPRC99 chemical mechanism (Carter, 2000). CAMx simulates emission, advection, dispersion, chemical transformation and physical removal of air pollutants on an Eulerian 3-dimensional grid. The 6 modeling episodes selected for this study are described in Sect. 2.3 along with their meteorological classification. A gridded urban

Title Page

Abstract

Introduction

Conclusions

References

Tables

Figures

◀

▶

◀

▶

Back

Close

Full Screen / Esc

Printer-friendly Version

Interactive Discussion



scale domain centering in Mexico City with the resolution of 3 km, 70×70 grid cells was used in this study (labeled as “modeling domain” in Fig. 1) with 16 vertical layers extending from the surface to about 7 km a.g.l.

Meteorological data inputs, including wind, temperature, height/pressure, water vapor, vertical diffusivity, and clouds/precipitation, were derived from the Advanced Research WRF (ARW) model (WRF v2.2.1; Skamarock et al., 2005). The model simulations adopted three one-way nested grids with horizontal resolutions of 36, 12, and 3 km and 35 sigma levels in the vertical direction. The grid cells used for the three domains were 145×95, 259×160, and 193×193, respectively. The WRF model was initialized at 00:00 UTC every day and integrated for 36 h. The physical parameterization schemes included the modified Kain-Fritsch cumulus scheme (KF-Eta; Kain and Fritsch, 1993), the WRF Single Moment (WSM) three-class microphysics (Hong et al., 2004), and the Yonsei State University (YSU) boundary layer scheme (Noh et al., 2003). National Centers for Environmental Prediction (NCEP) global final (FNL) analysis were used to create initial and boundary conditions. To improve the accuracy of the simulated fields, “observation-nudging”-based continuous four-dimensional data assimilation (FDDA) scheme (WRF-FDDA; Liu et al., 2005) was employed in the domain with a horizontal resolution of 3 km. Multi-level upper-air observations were assimilated, including radar wind profilers, tethered balloon measurements, controlled meteorological balloon observations, aircraft observations, additional soundings inside the Mexico city basin operated during the MILAGRO campaign, and routine soundings observations. The vertical diffusion coefficients ( $k_v$ ) were reconstructed from the state variables of the WRF-FDDA output using the CMAQ scheme (Byun, 1999). According to de Foy et al. (2008), the CMAQ scheme overestimates the  $k_v$  values. These were therefore reduced to 30–40% as was done for the MCMA-2003 campaign (see Lei et al., 2008). This  $k_v$  scaling has little influence on chemical concentrations at nighttime and early morning (because of the patch treatment for the minimum  $k_v$  values in the near surface layer), but it affects the day time concentrations (as much as 15% for surface CO) when there is active turbulent mixing.

**Ozone response to emission changes**

J. Song et al.

Title Page

Abstract

Introduction

Conclusions

References

Tables

Figures

◀

▶

◀

▶

Back

Close

Full Screen / Esc

Printer-friendly Version

Interactive Discussion



## Ozone response to emission changes

J. Song et al.

Title Page

Abstract

Introduction

Conclusions

References

Tables

Figures

◀

▶

◀

▶

Back

Close

Full Screen / Esc

Printer-friendly Version

Interactive Discussion



Anthropogenic emissions used in the model were constructed from the official emission inventory (EI) for the year 2006 for the MCMA ([http://www.sma.df.gob.mx/simat/programas\\_ambientales/anexo](http://www.sma.df.gob.mx/simat/programas_ambientales/anexo)). The annual emissions in the MCMA from different sources (mobile, area, and point source) were temporally resolved, chemically speciated, and then spatially resolved into grid cells with a resolution of 2.25 km. In areas outside the MCMA, official emissions data from point sources were available, but area and mobile emissions were not available. To account for these emissions, anthropogenic emissions outside the MCMA from the area and mobile sources were estimated based on the population distribution as follows:

$$E_{i,j} = r_j \times \frac{E_{j,MCMA}}{P_{MCMA}} \times SF \quad (1)$$

where  $r_j$  is population density in the grid cell obtained from a high resolution population density map in the year of 2005,  $E_{j,MCMA}$  and  $P_{MCMA}$  are the total anthropogenic emissions of pollutant  $j$  and the population in the MCMA, respectively. SF are the population-based scaling factors that account for differences in emission intensities with respect to the MCMA, ranging linearly from 0.1 to 0.3 for  $r < 200$  heads/km<sup>2</sup> (mainly rural areas) and  $r < 15000$  heads/km<sup>2</sup> (mainly urban areas with much higher production activities). Lei et al. (2007, 2008) suggested that the overall VOC emissions in the official MCMA EI were underestimated by 40% with variations among VOC species. Based on the ground measurements made at CENICA site and at T0, adjustments were made to the emissions of lumped VOCs species (see Sect. 3.1 below). When the measurements were unavailable, adjustment factors from the MCMA-2003 study were used.

Biogenic emissions were estimated using the MEGAN v2.04 model (Model of Emissions of Gases and Aerosols from Nature) developed by Guenther et al. (2006, 2007). MEGAN uses land cover data with a high resolution (less than 1 km), emission factors specific to the interested region, and time- and location-specific meteorological data. MEGAN estimates biogenic emissions as follows:

$$F = EF \cdot \gamma_{LAI} \cdot \gamma_P \cdot \gamma_T \cdot \gamma_{AGE} \quad (2)$$

where  $F$  is the emission flux ( $\mu\text{gm}^{-2}\text{h}^{-1}$ ),  $EF$  is the emission factor at standard condition of 303 K ( $\mu\text{gm}^{-2}\text{h}^{-1}$ ),  $\gamma_{\text{LAI}}$ ,  $\gamma_P$ ,  $\gamma_T$ , and  $\gamma_{\text{AGE}}$  are dimensionless scalars that describe the response of emission to diurnal variation in leaf area index (LAI), photosynthetic photon flux density (PPFD), ambient temperature, and leaf age, respectively.

The emissions estimated from MEGAN on the spatial resolution of 1 km were then lumped into the SAPRC99 species groups.

### 2.3 Meteorological episodes

$\text{O}_3$  production under different meteorological conditions was examined. During MCMA-2003, three meteorological episode types were identified (de Foy et al., 2005).  $\text{O}_3$ -South days had a convergence zone in the south of the city that moved northwards into the early evening, causing high ozone peaks in the south of the city.  $\text{O}_3$ -North days had stronger westerly winds aloft causing a convergence zone oriented north-south through the city with pollutant exhaust to the north and high ozone peaks in the north. Cold Surge days had strong cold and wet winds from the north flushing the basin to the south, bringing rain and cloudiness with them.

During MILAGRO, six meteorological episode types were identified: the same three as during MCMA-2003, and an extra three to account for conditions at the beginning and at the end of the campaign (de Foy et al., 2008). The first part of the campaign had northwesterly winds aloft with strong southward transport at the surface and no convergence zones in the basin. These “South-Venting” days had clean air and rapid flushing of the urban plume to the south. The second part of the campaign was characterized by afternoon rains. These were classified into two subtypes depending on the location of the maximum amount of rainfall: Convection-South and Convection-North. Convection takes place when there are weak westerly winds aloft combined with humid conditions in the basin. Surface convergence in the afternoon leads to convection and rainfall in the basin with the location to the north or south dependent on the balance of the winds from the plateau to the north and from the gap in the southeast. Cluster

## Ozone response to emission changes

J. Song et al.

Title Page

Abstract

Introduction

Conclusions

References

Tables

Figures

◀

▶

◀

▶

Back

Close

Full Screen / Esc

Printer-friendly Version

Interactive Discussion



**Ozone response to emission changes**

J. Song et al.

[Title Page](#)[Abstract](#)[Introduction](#)[Conclusions](#)[References](#)[Tables](#)[Figures](#)[I◀](#)[▶I](#)[◀](#)[▶](#)[Back](#)[Close](#)[Full Screen / Esc](#)[Printer-friendly Version](#)[Interactive Discussion](#)

analysis of radiosonde profiles and surface wind measurements showed that conditions during MILAGRO were climatologically representative of the warm dry season, suggesting that an analysis of O<sub>3</sub> production during the different episodes of MILAGRO would be representative of general conditions in the basin for this season (de Foy et al., 2008).

To minimize the influence from the transition of different meteorological conditions on the selected episode, each episode was selected when at least 3 consecutive days had similar meteorological condition: 1–7 March 2006 as O<sub>3</sub>-South Venting (O<sub>3</sub>-SV), 9–11 March 2006 as O<sub>3</sub>-North (O<sub>3</sub>-N1), 15–17 March 2006 as O<sub>3</sub>-South (O<sub>3</sub>-S), 18–20 March 2006 as O<sub>3</sub>-North (O<sub>3</sub>-N2), 24–26 March 2006 as O<sub>3</sub>-Convection South (O<sub>3</sub>-CnvS), and 27–30 March 2006 as O<sub>3</sub>-Convection North (O<sub>3</sub>-CnvN). O<sub>3</sub>-N1 was a period with flow towards the north and included one of the highest ozone days (11 March), and the O<sub>3</sub>-N2 was a holiday period.

Mexico City was in the Central Standard Time zone at the time of the campaign (CST=UTC–6); all results in this paper will be reported in local time (LT=CST).

### 3 Results and discussions

Simulations of 1-h averaged ozone precursors and ozone concentrations using CAMx v4.40 were compared to measurements made during different meteorological episodes. A day prior to each modeled episode was used for model “spin-up”, so that results of these days are not included.

#### 3.1 Adjustment of emission inventory

For ozone precursors and ozone, simulations with the official emission inventory were compared with the measurements taken from 15 RAMA monitoring sites, the CENICA site and the T0 supersite. Figure 2 shows that peak CO and NO<sub>y</sub> concentrations were well simulated, with no mean fractional bias and low fractional errors (see definitions

**Ozone response to emission changes**

J. Song et al.

Title Page

Abstract

Introduction

Conclusions

References

Tables

Figures

◀

▶

◀

▶

Back

Close

Full Screen / Esc

Printer-friendly Version

Interactive Discussion



below), suggesting that no adjustments to the emission inventory were necessary for these species. Analysis of speciated VOC concentrations suggested that emissions of most alkanes were underestimated by factors of 2–3 in mass except the ones with high OH reactivity (ALK4, ALK5), whereas emissions of aromatics were overestimated by a factor of 2. Ethylene (ETHE) emissions were underestimated by 40% while emissions of other olefins were overestimated by up to 50%. Also, emissions of aldehydes were underestimated by factors of 3–4.5. Figure 3 compares VOC concentrations simulated using emissions adjusted for the above underestimates/overestimates with the observed values at CENICA and T0. The statistical metrics shown in the figure, mean fractional bias (MFB) and mean fractional error (MFE), are defined as Metrics are defined as

$$\text{Mean fractional bias (MFB)} = \frac{1}{N} \sum_1^N \left( \frac{\text{pred} - \text{obs}}{(\text{pred} + \text{obs})/2} \right) \times 100\% \quad (3)$$

$$\text{Mean fractional error (MFE)} = \frac{1}{N} \sum_1^N \left( \frac{|\text{pred} - \text{obs}|}{(\text{pred} + \text{obs})/2} \right) \times 100\% \quad (4)$$

where  $N$  is the number of observations. In contrast with mean normalized bias (MNB) and mean normalized gross error (MNGE) statistical metrics, MFB and MFE do not put great emphasis on performance when observations are low (Boylan and Russell, 2006).

After the emissions were adjusted, the agreement between simulated and observed VOCs was within  $\pm 1$  standard deviation. It should be noted that some VOCs, for example HCHO and ETHE, measured concurrently and independently by different groups at the same site showed large variations (Fig. 3e and f). The difference can be partially explained by the different temporal coverage of the different measurements. Nevertheless, it may suggest that the emissions of ETHE and HCHO may require further analysis. Mean values of the measurements for these two lumped species by different groups were used for the emission adjustments of these species in our modeling. The

post-adjusted ARO<sub>2</sub> emissions seem to be still underestimated by 15%.

The measurement data at SIMAT were not included during the emission adjustment process (they were not available when we completed the model runs), instead they were used to verify the adjustment. Figure 4 shows the comparison of the simulated propene-equivalent olefin concentrations with the FOS measurements. The simulated effective OLE concentrations were calculated from different OLE model species (ETHE, OLE1, OLE2 and ISOP) weighted by their FOS response factors and their contributions to the standard VOC mixture used in the SAPRC99 mechanism (Lei et al., 2009; Velasco et al., 2009). The good agreement justifies the adjustment of olefin emissions.

A summary of total weekday emissions by source category in MCMA from 2006 official emission inventory and the adjusted emissions are listed in Table 2. Overall, the VOC emissions from the official emission inventory were adjusted by 18–23% with the variability depending on the day-to-day variation in biogenic emissions. These variations are even more significant on the domain-wide emissions, leading to larger variations in overall total VOC emissions. The total VOC adjustment in the MCMA is smaller than the value used by Lei et al. (2007, 2008) (1.26 vs. 1.65), probably due to the VOC emissions changes over the years in both the emission inventories and in actual emissions. Zavala et al. (2009) find that the mobile emission factors of a few VOC species (mainly aldehydes and aromatics) are reduced between 2003 and 2006 in the MCMA (by about 20%). Although the measured VOC species are only a small portion of the total VOCs, and the reported quantity is the emission factor, it may be a strong indication of the emissions reduction of VOCs in 2006 compared to 2003. It should be noted that there are no sufficient VOC measurements available to reach a quantitative conclusion about the VOC emission changes between 2003 and 2006. The size of the VOC measurement dataset for evaluation and the variability in measurements may also contribute to the difference.

The adjusted emissions (base case) of CO, NO<sub>x</sub> and VOCs in the MCMA-2006 are 1990, 195 and 700–743 ktons/yr, respectively. Compared to those of MCMA-2003, which are 1938, 183 and 900 ktons/yr (Lei et al., 2007, 2008), the NO<sub>x</sub> emissions in-

**Ozone response to emission changes**

J. Song et al.

[Title Page](#)[Abstract](#)[Introduction](#)[Conclusions](#)[References](#)[Tables](#)[Figures](#)[◀](#)[▶](#)[◀](#)[▶](#)[Back](#)[Close](#)[Full Screen / Esc](#)[Printer-friendly Version](#)[Interactive Discussion](#)

creased slightly (6%), but the VOCs emissions decreased by about 20%, leading to the  $\text{NO}_x/\text{VOC}$  ratio changes from 4.9 in 2003 to 3.7 (mass-based) in 2006. In addition, the total emissions of highly reactive VOCs (alkenes and aromatics) decrease significantly, resulting in the reduction of VOC reactivity in 2006 compared to 2003. These changes in the  $\text{VOC}/\text{NO}_x$  ratio and VOC reactivity in 2006 could affect the characteristics of ozone formation in the MCMA. For example, the lower  $\text{VOC}/\text{NO}_x$  ratio and lower VOC reactivity may contribute to the lower radical levels observed during the MCMA-2006 campaign compared to MCMA-2003 (Shirley et al., 2006; Dusanter et al., 2009a,b).

### 3.2 Simulation of ozone precursors and ozone concentrations at surface

Before a model can be applied for  $\text{O}_3$  sensitivity studies it is essential to demonstrate its capability to accurately simulate the observations. We now compare simulations and concentrations of ozone and ozone precursors both at ground level and aloft.

As depicted in Fig. 5, the observed concentrations of ozone were well reproduced by the model except for a few days, 4, 11, and 25 March 2006 which are all Saturdays. On 4 and 11 March, the spatial distribution of ozone concentrations showed that the location of the plume was accurately simulated, but the simulated magnitude was much lower (figures not shown). This might be because emissions on Saturdays were reduced by 15% in the simulations. Data analysis suggests that peak concentrations of primary pollutants may be lower on Saturdays, but the overall emissions may be similar to week days (Stephens et al., 2008; Stremme et al., 2009). On 25 March, the peak hours were not captured by the model, which might be due to the meteorology.

Differences of ozone profiles during different meteorological episodes can be explained by different wind patterns and characteristics of each episode. As southerly winds flushed out the basin during South-Venting days, and rain and high winds reduced photochemistry during Convection days, the observed ozone concentrations in the basin during these episodes were lower than those from other episodes (Fig. 5). During  $\text{O}_3\text{-S}$  and  $\text{O}_3\text{-N1}$ , on the other hand, pollutants accumulated in the south or north of the city which led to high observed ozone concentrations. Although  $\text{O}_3\text{-N1}$  and

## Ozone response to emission changes

J. Song et al.

Title Page

Abstract

Introduction

Conclusions

References

Tables

Figures

◀

▶

◀

▶

Back

Close

Full Screen / Esc

Printer-friendly Version

Interactive Discussion



**Ozone response to emission changes**

J. Song et al.

[Title Page](#)[Abstract](#)[Introduction](#)[Conclusions](#)[References](#)[Tables](#)[Figures](#)[◀](#)[▶](#)[◀](#)[▶](#)[Back](#)[Close](#)[Full Screen / Esc](#)[Printer-friendly Version](#)[Interactive Discussion](#)

O<sub>3</sub>-N2 fell into the same meteorological episode category, the daily maximum ozone concentrations averaged over RAMA sites differed by 40% (107 ppb during O<sub>3</sub>-N1 vs. 64 ppb during O<sub>3</sub>-N2 for episode-averaged peak ozone) mostly due to lower anthropogenic emissions (30–40% less) during the holiday period and also due to stronger southerly winds during O<sub>3</sub>-N2 that vented the pollutants more efficiently.

As shown in Fig. 2, simulated morning hours (07:00–11:00 LT) concentrations of CO and NO<sub>y</sub> agreed well with the observations. MFB and MFE during all the episodes were 2% and 16% for CO and were 1% and 17% for NO<sub>y</sub>. The agreements of ozone for all the episodes were fairly good with MFB and MFE values of –1% and 24%, respectively. Excluding weekend values, ozone concentrations showed better agreement with MFB and MFE values of –2% and 15%, respectively.

### 3.3 Comparisons with G-1 aircraft measurements

Two of the days when the G-1 aircraft flew over the urban area, 27 and 7 March, were selected as examples to compare the CO and ozone concentrations aloft. Good agreement between simulated and observed CO and O<sub>3</sub> concentrations at the surface (not shown) were obtained for both days. Figure 6 shows the G-1 flight path on both days with the overpass time at each supersite as well as starting and ending times of each flight. On 27 March, classified as O<sub>3</sub>-CnvN, the flight focused more on the northwestern MCMA and T1 supersite and traversed an elevated pollutant plume four times (location “A” in Fig. 6a). Simulated concentrations were interpolated in time and space to the time and location of the data along the flight track. Figure 7 shows the comparisons of O<sub>3</sub> and CO. The agreement between the model and the observations on March 27 was remarkably good, especially for O<sub>3</sub>, indicating the pollution plume was well captured by the model. On 7 March, classified as O<sub>3</sub>-SV, the plane flew over southwestern MCMA 5 times (Location “B” in Fig. 6b) and captured the high CO and O<sub>3</sub> concentrations between 13:06 and 14:09 LT. The measured plume width was about 15 km, whereas the simulated plume was about 28 km wide, which resulted in lower and longer-lasting elevated concentrations for both CO and O<sub>3</sub> (Fig. 7b). Although

quantitatively speaking the model did not simulate well the magnitude and width of the plume, qualitatively it captured both the location and the peak time. This was representative of other days where the simulated urban plumes were in qualitative agreement with the observations

5 The aircraft measurements on 27 March also provided speciated VOC data for further model evaluation. Figure 8 shows the comparison of simulated VOCs and observations along with the flight path. Agreement between simulated and observed VOCs was good, especially with ethene and alkanes. On the other hand, peak concentrations of ARO<sub>2</sub> were underpredicted, consistent with the underestimation indicated by  
10 T<sub>0</sub> comparison (Fig. 3d), suggesting that the ARO<sub>2</sub> emissions may need to be improved. However, the underestimate of emissions (15%) is not adequate to explain the significant underprediction of ARO<sub>2</sub>. This may also imply that the modeled plume is possibly chemically over-active such that most of the highly active ARO<sub>2</sub> is chemically lost in lower altitudes (note that the pollution plume is well captured by the model).

15 In summary the model qualitatively and to some extent quantitatively captured the urban plume; this indicates that the model represents the main features of the transport and mixing processes, as well as the interaction of emission, transport and chemistry. Together with the excellent agreement of the near-surface concentrations, this provides further confidence in the model's ability to simulate ozone concentrations, which  
20 provides a viable case from which to proceed with the O<sub>3</sub> sensitivity investigation.

### 3.4 Characteristics of ozone formation during the MCMA-2006 Field Campaign

#### 3.4.1 Ozone formation and its sensitivity to emissions

25 Relationships among net photochemical formation rate ( $P(O_x)$ ), where  $O_x$  is defined as  $O_3 + NO_2$ , radical primary sources ( $Q$ ), and  $NO_x$  oxidation rate ( $P(NO_z)$ ) help to determine if the  $O_3$  formation is in a VOC- or  $NO_x$ -limited regime. Analysis limiting the data between 12:00 and 17:00LT during each episode period within the urban

## Ozone response to emission changes

J. Song et al.

Title Page

Abstract

Introduction

Conclusions

References

Tables

Figures

◀

▶

◀

▶

Back

Close

Full Screen / Esc

Printer-friendly Version

Interactive Discussion



**Ozone response to emission changes**

J. Song et al.

[Title Page](#)[Abstract](#)[Introduction](#)[Conclusions](#)[References](#)[Tables](#)[Figures](#)[◀](#)[▶](#)[◀](#)[▶](#)[Back](#)[Close](#)[Full Screen / Esc](#)[Printer-friendly Version](#)[Interactive Discussion](#)

area is presented in Fig. 9. As shown in Fig. 9,  $O_x$  formation is largely determined by the available radical sources (Fig. 9a), and the reaction of radicals with  $NO_x$  is the dominant radical sink regardless of meteorological conditions (Fig. 9b), which implies that the reactions of OH radicals with VOCs in the urban area are the rate-limiting step for  $O_3$  formation (Daum et al., 2000; Kleinman et al., 1997; Kleinman, 2005; Sillman, 1995). The mean  $O_x$  production efficiency derived from Fig. 9 is 7, which is in good agreement with the measurement-based estimates of 7 by Wood et al. (2009) in the urban area during the MCMA-2006 campaign.

The effects of reducing precursor emissions were analyzed for three representative emission control strategies: 50% reduction in total VOC emissions (50% VOC), 50% reduction in total  $NO_x$  emissions (50%  $NO_x$ ), and 50% reduction in both VOC and  $NO_x$  emissions (50% All). The results are shown in Fig. 10 and Table 3. For the base case, peak ozone concentrations averaged over the 15 RAMA monitoring sites occurred at 13:00–15:00 LT depending on the episode. A 50% reduction in VOC emissions led to 11.8–30.7 ppb (16.6–32.8%) decrease in peak  $O_3$  concentrations averaged over the 15 monitoring sites in the MCMA, varying with episodes, while a 50% reduction in  $NO_x$  emissions led to 6.5–31.8 ppb (9.2–37.7%) increase in the peak averages, and 50% reductions in both VOC and  $NO_x$  emissions led to 4.9–13.3 ppb (6.8–14.2%) decrease in the peak averages. Both the absolute and relative changes are larger than obtained during MCMA-2003 (Lei et al., 2007, 2008), mainly due to the changes in estimated VOC emissions. The ozone concentrations from 50% VOC followed the trend of the base case in the early morning and late afternoon; however, daytime ozone concentrations were significantly lower than those from the base case. Also, peak ozone concentrations from 50% VOC reduction generally occurred 1–2 h later than those from the base case. On the other hand,  $NO_x$  reductions produced significant increases in peak ozone throughout the day, and peak ozone concentrations occurred 1–2 h earlier than those from the base case. Reductions in both VOC and  $NO_x$  emissions generally followed the trend of the base case during the daytime with changes in episode-averaged daily maximum 1-h ozone concentrations (4.9 ppb decrease from  $O_3$ -N2 to 13.3 ppb

decrease from O<sub>3</sub>-N1), but followed the trend of 50% NO<sub>x</sub> in the early morning and late afternoon.

During different meteorological episodes, the magnitude of changes, as well as the peak ozone timing was different for different emission control scenarios, with the largest changes in the O<sub>3</sub>-S episode and the smallest changes during the convection events. These results suggest that the MCMA urban region is VOC-limited during the ozone peak hours as well as during the morning and late afternoon. Under VOC-limited conditions, ozone formation is limited by the amount of available radicals for NO → NO<sub>2</sub> conversion (RO<sub>2</sub>/HO<sub>2</sub>+NO → RO/OH+NO<sub>2</sub>) that eventually leads to O<sub>3</sub> production. Meanwhile NO<sub>2</sub>-radical reactions become the dominant radical chemical sink. These findings are consistent with results from the MCMA-2003 field campaign (Lei et al., 2007, 2008; Volkamer et al., 2007; Sheehy et al., 2008) as well as with MILAGRO measurement-based conclusions (Nunnermacker et al., 2008; Wood et al., 2008; Stephens et al., 2008).

Figure 11 shows the spatial distribution of changes in peak ozone concentrations due to reductions in emissions of VOCs, NO<sub>x</sub>, and both during each meteorological episode. Compared to the base case, 50% reductions in VOC emissions led to domain-wide decrease in ozone concentrations, up to 55.8 ppb (Fig. 11b). These reductions were apparent in the regions where peak ozone concentrations were simulated. In contrast, 50% reductions in NO<sub>x</sub> emissions led to either increases or decreases in peak ozone concentrations, depending on the location (Fig. 11c). In the urban area, ozone concentrations increased by up to 56.3 ppb due to the reductions in NO<sub>x</sub> emissions while they decreased in mountain/rural areas. The spatial distributions of changes in ozone concentrations were also sensitive to the direction of the plume, which was highly dependent on the meteorological episode. When both VOC and NO<sub>x</sub> emissions were reduced, ozone concentrations in the urban area either increase or decrease depending on the direction of the plume (Fig. 11d). For example, ozone concentrations at peak hours during O<sub>3</sub>-N1 decreased by up to 26.0 ppb in the urban area when both VOC and NO<sub>x</sub> emissions were reduced; however, the concentration at the same lo-

**Ozone response to emission changes**

J. Song et al.

[Title Page](#)[Abstract](#)[Introduction](#)[Conclusions](#)[References](#)[Tables](#)[Figures](#)[I◀](#)[▶I](#)[◀](#)[▶](#)[Back](#)[Close](#)[Full Screen / Esc](#)[Printer-friendly Version](#)[Interactive Discussion](#)

cation increased by up to 6.9 ppb during O<sub>3</sub>-CnvS. This further suggests that ozone formation in the MCMA urban area is VOC-sensitive.

### 3.4.2 Indicator ( $P_{\text{H}_2\text{O}_2}/P_{\text{HNO}_3}$ ) analysis

The ratio of the production rates of hydrogen peroxide and nitric acid ( $P_{\text{H}_2\text{O}_2}/P_{\text{HNO}_3}$ ) has been widely used in chemical indicator analysis to examine the sensitivity of ozone formation (Sillman, 1995; Tonnesen and Dennis, 2000). It has been established in many urban areas in North America that if the  $P_{\text{H}_2\text{O}_2}/P_{\text{HNO}_3}$  ratio is 0.35 and higher, it is defined as NO<sub>x</sub>-limited regime; if the ratio is 0.06 and lower, it is defined as VOC-limited regime, and in between it is defined as a transition regime. Figure 12a depicts the relationships between  $P(\text{O}_x)$  and  $P_{\text{H}_2\text{O}_2}/P_{\text{HNO}_3}$  at 12:00–17:00 LT under two different emission reduction scenarios: 50% VOC and 50% NO<sub>x</sub>. During different meteorological episodes, the ozone formation is NO<sub>x</sub>-limited when the  $P_{\text{H}_2\text{O}_2}/P_{\text{HNO}_3}$  ratio is 0.28 and higher, VOC-limited when the ratio is 0.1 and lower, and transitional when the ratio is between 0.10 and 0.28. These results are within the criteria that were specified from previous studies (Sillman, 1995; Tonnesen and Dennis, 2000). Note that Fig. 12a encompasses all the episodes including weekends (shown in gray). Most gray data points overlapped with other data points, indicating that the relationship between  $P(\text{O}_x)$  and  $P_{\text{H}_2\text{O}_2}/P_{\text{HNO}_3}$  during weekends is the same as the one during weekdays.

The  $P_{\text{H}_2\text{O}_2}/P_{\text{HNO}_3}$  criteria were applied to examine the spatial distribution of VOC and NO<sub>x</sub> limitations. Figure 12b gives an example of the  $P_{\text{H}_2\text{O}_2}/P_{\text{HNO}_3}$  spatial variation on 7 and 27 March, two days with a high percentage of VOC- and NO<sub>x</sub>-limited regime, respectively. As shown in the figure, there is a large variation in the spatial distributions of VOC- or NO<sub>x</sub>-limited regime in the afternoon among different meteorological episodes: ozone formation in the high NO<sub>x</sub> emitting urban areas are sensitive to VOC, whereas the ozone formations in the mountains or low NO<sub>x</sub> emitting rural areas are more sensitive to NO<sub>x</sub>. In terms of the urban area, controlling VOCs would be a more effective way to reduce ozone concentrations than controlling NO<sub>x</sub>; however, it is essential to

## Ozone response to emission changes

J. Song et al.

Title Page

Abstract

Introduction

Conclusions

References

Tables

Figures

◀

▶

◀

▶

Back

Close

Full Screen / Esc

Printer-friendly Version

Interactive Discussion



understand that the sensitivity of VOC- or NO<sub>x</sub>-limited regime changes over time and space.

Lei et al. (2007, 2008) show that the O<sub>3</sub> sensitivity in the MCMA is closely related to chemical aging (NO<sub>z</sub>/NO<sub>y</sub>) of the urban plume, and point out that as the plume becomes chemically aged the O<sub>3</sub> formation tends to shift from VOC-limited to NO<sub>x</sub>-limited, but no criteria are established for the transition. In this study, we attempt to establish criteria by analyzing the  $P(O_x)$ -NO<sub>z</sub>/NO<sub>y</sub> relationship under different emissions, in order to use measurements to assess the O<sub>3</sub> formation regime. Figure 13 illustrates the percentage change in  $P(O_x)$  ( $\Delta P(O_x)$ ) as a function of base case NO<sub>z</sub>/NO<sub>y</sub> at 12:00–17:00 LT in the MCMA urban region under different meteorological conditions during the MILAGRO campaign when emissions are reduced by 50%. Figure 13a–f shows the change on weekdays while Fig. 13g shows the change during weekends. We find that  $\Delta P(O_x)$  generally decreases with increasing chemical aging and shifts from positive to negative when the NO<sub>x</sub> emissions are reduced by 50%,  $\Delta P(O_x)$  increases gradually with increasing NO<sub>z</sub>/NO<sub>y</sub> when the VOC emissions are reduced by 50%, while  $\Delta P(O_x)$  remains constant with NO<sub>z</sub>/NO<sub>y</sub> when emissions of both NO<sub>x</sub> and VOCs are reduced by 50%. These characteristics are consistent under different meteorological conditions, and no noticeable differences are found between weekdays and weekends. Furthermore, it can be established that O<sub>3</sub> formation is VOC-limited when NO<sub>z</sub>/NO<sub>y</sub> < 0.45, but is NO<sub>x</sub>-limited when NO<sub>z</sub>/NO<sub>y</sub> > 0.60, with the latter occurring significantly less frequently. It should be noted that these criteria may change with location and with different base emissions. For example, a Lagrangian-wise analysis by Lei et al. (2008) shows that the urban plume becomes NO<sub>x</sub>-limited when NO<sub>z</sub>/NO<sub>y</sub> > 0.8 after the plume travels outside of the MCMA urban area during the MCMA-2003 campaign.

### 3.5 Comparison of findings with the MCMA-2003 Field Campaign

During MCMA-2003 field campaign, the relationships between ozone production rate, radical primary source, and VOC-to-NO<sub>2</sub> reactivity showed that the urban core area were VOC-limited during the O<sub>3</sub>-South, Cold-Surge, and O<sub>3</sub>-North episodes. This was

## Ozone response to emission changes

J. Song et al.

Title Page

Abstract

Introduction

Conclusions

References

Tables

Figures

◀

▶

◀

▶

Back

Close

Full Screen / Esc

Printer-friendly Version

Interactive Discussion



**Ozone response to emission changes**

J. Song et al.

[Title Page](#)[Abstract](#)[Introduction](#)[Conclusions](#)[References](#)[Tables](#)[Figures](#)[I◀](#)[▶I](#)[◀](#)[▶](#)[Back](#)[Close](#)[Full Screen / Esc](#)[Printer-friendly Version](#)[Interactive Discussion](#)

further analyzed by the simulations using three different emissions control strategies. Similar findings were obtained during the MCMA-2006 field campaign under different meteorological conditions. However, the degree of the VOC limitation increases as shown in Figs. 10 and 13. The  $\Delta P(\text{O}_x)$ – $\text{NO}_x$  relationship shown in Fig. 14 also indicates that the transition area between VOC-sensitive and  $\text{NO}_x$ -sensitive regimes is much more narrow and shifts to lower  $\text{NO}_x$  levels in MCMA-2006 compared to the MCMA-2003, and the relationship for the  $\text{NO}_x$ -reduction case is more monotonic. These illustrate that  $\text{O}_3$  formation in the urban area during the MCMA-2006 is more VOC-limited, which is due to reduced VOC/ $\text{NO}_x$  ratio and VOC reactivity in the estimated emissions. Although not shown in Fig. 14 (because almost all weekend data points would be overlapped with the weekdays counterparts), the  $\text{O}_3$  formation response to the emission change is very similar to that of weekdays, consistent with the results using  $P(\text{H}_2\text{O}_2)/P(\text{HNO}_3)$  ratio as indicator. On the other hand, although the ozone formations in the urban area were VOC-limited regardless of the meteorological episodes, it was also suggested that areas outside the city with relatively low- $\text{NO}_x$  emissions could be both  $\text{NO}_x$ - or VOC-limited regime depending on the meteorological episode.

## 4 Conclusions

We have extended the MCMA-2003 study of Lei et al. (2007, 2008) to the MCMA-2006 field campaign using CAMx v4.4 that was driven by observation-budged WRF meteorology. This study not only examined more meteorological episodes, but also encompassed a wider region with updated emissions. Several major questions were addressed under different meteorological condition.

Due to uncertainties in the emission inventory, emissions of  $\text{CO}$ ,  $\text{NO}_x$ , and VOCs were compared to the measurements from air quality monitoring sites and from the MCMA-2006 field campaign. Simulations with  $\text{CO}$  and  $\text{NO}_x$  emissions from the official 2006 emission inventory agreed well with the observations, while emissions of

5 speciated VOCs required further adjustments. Overall, total VOC emissions were underestimated by 18–23% which is much smaller than the results found in Lei et al. (2007, 2008). With adjusted emissions, simulated ozone precursors and ozone concentrations were compared to observations from a variety of measurements, including surface measurements and aircraft measurements, under different meteorological episodes. Except for a few days, the observed concentrations of ozone and ozone precursors at the surface were well reproduced by the model. The peaks from aircraft measurements were also well reproduced by the model. The combination of surface and aircraft measurements allow the evaluation of the simulated vertical distribution of CO, VOC, and O<sub>3</sub> concentrations as well as an evaluation of the local emission inventory.

To determine the relative benefits of VOC and NO<sub>x</sub> controls, we have examined the relationships among net photochemical formation rates, radical primary sources, and NO<sub>x</sub> oxidation rates in the MCMA urban area. We also have examined the ratio of the production rates of hydrogen peroxide and nitric acid,  $P_{\text{H}_2\text{O}_2}/P_{\text{HNO}_3}$  in the urban area and mountain/rural areas. Within the urban area, O<sub>x</sub> formation was largely determined by the radical sources available, and the reaction of radicals with NO<sub>x</sub> represented the dominant radical sink, which implied that the urban area is VOC-sensitive regardless of meteorological conditions. This was also shown from the spatial distribution of  $P_{\text{H}_2\text{O}_2}/P_{\text{HNO}_3}$ . In contrast, ozone formation in the mountain areas or low NO<sub>x</sub> emitting rural areas was mostly NO<sub>x</sub>-limited depending on meteorological conditions.

We have also examined the sensitivities of ozone production to precursor emissions during the MCMA-2006 field campaign. Regardless of different meteorological episodes, reductions in VOC emissions led to domain-wide decrease in ozone concentrations at the regions where peak ozone concentrations were simulated. In contrast, reductions in NO<sub>x</sub> emissions led to large increases in the urban area and decreases in mountain/rural areas. However, spatial distributions of changes in ozone concentrations were highly sensitive to the meteorological episode. This was more evident when both VOC and NO<sub>x</sub> emissions were reduced because ozone concentrations in

**Ozone response to emission changes**

J. Song et al.

[Title Page](#)[Abstract](#)[Introduction](#)[Conclusions](#)[References](#)[Tables](#)[Figures](#)[◀](#)[▶](#)[◀](#)[▶](#)[Back](#)[Close](#)[Full Screen / Esc](#)[Printer-friendly Version](#)[Interactive Discussion](#)

the urban area experienced both increase and decrease depending on the direction of the plume.

Overall, ozone formation in the urban core area was VOC-limited under different meteorological episodes, while the surrounding areas with relatively low-NO<sub>x</sub> emissions can be either NO<sub>x</sub>- or VOC-limited regime depending on the episode. Our results from MCMA-2006 suggest that the controls on VOC emissions would be a more effective way to reduce ozone concentrations in the urban area, which is consistent with our previous results from the MCMA-2003 field campaign. However, the degree of VOC-limitation increased for MCMA-2006 due to reduced VOC/NO<sub>x</sub> ratio and VOC reactivity in the estimated emissions. Furthermore, meteorological conditions led to large variations in regime for the relatively low-NO<sub>x</sub> emitting area, implying that emission controls would depend on location and meteorology. Finally, it is the urban area near the surface that is VOC-limited; the situation could be different aloft. Spencer et al. (2009) argues that if missing radical sources are accounted for, O<sub>3</sub> production over the MCMA (below 7 km a.s.l.) could be NO<sub>x</sub>-limited or the regime may shift to NO<sub>x</sub>-limited at higher NO<sub>x</sub> levels.

*Acknowledgements.* We are indebted to the large number of people involved in the MILAGRO campaign as well as those involved in long-term air quality monitoring and the emissions inventory in the Mexico City metropolitan area, which made this study possible. In particular, we are grateful to Christine Wiedinmyer for her assistance with the MEGAN simulations, the Government of the Federal District for providing point emissions data outside of the MCMA; the researchers from the University of California at Irvine, Aerodyne Research Inc., Washington State University, BNL and PNNL for making their data available to constrain our chemical transport model The WRF computer time was provided by the National Center for Atmospheric Research, which is sponsored by the National Science Foundation. This work was supported by the US Department of Energy's Atmospheric Sciences Program (DE-FG02-05ER63980), the US National Science Foundation's Atmospheric Chemistry Program (ATM-0528227 and ATM-810931), Mexico's Comisión Ambiental Metropolitana and the Molina Center for Energy and the Environment.

**Ozone response to emission changes**

J. Song et al.

[Title Page](#)[Abstract](#)[Introduction](#)[Conclusions](#)[References](#)[Tables](#)[Figures](#)[◀](#)[▶](#)[◀](#)[▶](#)[Back](#)[Close](#)[Full Screen / Esc](#)[Printer-friendly Version](#)[Interactive Discussion](#)

## References

- Apel, K. T., Flocke, F., Hills, A. J., Emmons, L., Madronich, S., Fried, A., Tie, X., Mauldin, L., Campos, T., Sive, B., Kleinman, Springston, L., Ortega, S., Blake, J. D., Baker, A., Warneke, C., Welsh-Bon, D., de Gouw, J., Zheng, J., Zhang, R., Rudolph, J., Junkermann, W., and Riemer, D. D.: Characterization of volatile organic compounds in the Mexico City Metropolitan area and in the outflow from the city, submitted to Atmos. Chem. Physics. Discuss., 2009.
- Boylan, J. W. and Russell, A. G.: PM and light extinction model performance metrics, goals, and criteria for three-dimensional air quality models, Atmos. Environ., 40, 4946–4959, 2006.
- Byun, D. W.: Dynamically consistent formulations in meteorological and air quality models for multiscale atmospheric studies. Part I: Governing equations in a generalized coordinate system, J. Atmos. Sci., 56, 3789–3807, 1999.
- Carter, W.: Implementation of the SAPRC-99 chemical mechanism into the Models-3 framework. Report to the United States Environmental Protection Agency, online available at: <http://www.cert.ucr.edu/~carter/absts.htm#s99mod3>, 29 January, 2000,.
- Daum, P. H., Kleinman, L., Imre, D. G., Nunnermacker, L. J., Lee, Y.-N., Springston, S. R., Newman, L., and Weinstein-Llyod, J.: Analysis of the processing of Nashville urban emission on July 3 and July 18, 1995, J. Geophys. Res., 105, 9155–9164, 2000.
- de Gouw, J. A., Welsh-Bon, D., Warneke, C., Kuster, W. C., Alexander, L., Baker, A. K., Beyersdorf, A. J., Blake, D. R., Canagaratna, M., Celada, A. T., Huey, L. G., Junkermann, W., Onasch, T. B., Salcido, A., Sjostedt, S. J., Sullivan, A. P., Tanner, D. J., Vargas, O., Weber, R. J., Worsnop, D. R., Yu, X. Y., and Zaveri, R.: Emission and chemistry of organic carbon in the gas and aerosol phase at a sub-urban site near Mexico City in March 2006 during the MILAGRO study, Atmos. Chem. Phys., 9, 3425–3442, 2009, <http://www.atmos-chem-phys.net/9/3425/2009/>.
- de Foy, B., Caetano, E., Magaña, V., Zitcuaro, A., Cárdenas, B., Retama, A., Ramos, R., Molina, L. T., and Molina, M. J.: Mexico City basin wind circulation during the MCMA-2003 field campaign, Atmos. Chem. Phys., 5, 2267–2288, 2005, <http://www.atmos-chem-phys.net/5/2267/2005/>.
- de Foy, B., Fast, J. D., Paech, S. J., Phillips, D., Walters, J. T., Coulter, R. L., Martin, T. J., Pekour, M. S., Shaw, W. J., Kastendeuch, P. P., Marley, N. A., Retama, A., and Molina, L. T.: Basin-scale wind transport during the MILAGRO field campaign and comparison to

### Ozone response to emission changes

J. Song et al.

Title Page

Abstract

Introduction

Conclusions

References

Tables

Figures

◀

▶

◀

▶

Back

Close

Full Screen / Esc

Printer-friendly Version

Interactive Discussion



climatology using cluster analysis, *Atmos. Chem. Phys.*, 8, 1209–1224, 2008,  
<http://www.atmos-chem-phys.net/8/1209/2008/>.

Dusanter, S., Vimal, D., Stevens, P. S., Volkamer, R., and Molina, L. T.: Measurements of OH and HO<sub>2</sub> concentrations during the MCMA-2006 field campaign – Part 1: Deployment of the Indiana University laser-induced fluorescence instrument, *Atmos. Chem. Phys.*, 9, 1665–1685, 2009a,  
<http://www.atmos-chem-phys.net/9/1665/2009/>.

Dusanter, S., Vimal, D., Stevens, P. S., Volkamer, R., Molina, L. T., Baker, A., Meinardi, S., Blake, D., Sheehy, P., Merten, A., Zhang, R., Zheng, J., Fortner, E. C., Junkermann, W., Dubey, M., Rahn, T., Eichinger, B., Lewandowski, P., Prueger, J., and Holder, H.: Measurements of OH and HO<sub>2</sub> concentrations during the MCMA-2006 field campaign – Part 2: Model comparison and radical budget, *Atmos. Chem. Phys.*, 9, 6655–6675, 2009b,  
<http://www.atmos-chem-phys.net/9/6655/2009/>.

ENVIRON: Users Guide to the Comprehensive Air Quality Model with Extensions (CAMx) version 4.40, online available at: <http://www.camx.com>, 2006.

Fortner, E. C., Zheng, J., Zhang, R., Berk Knighton, W., Volkamer, R. M., Sheehy, P., Molina, L., and André, M.: Measurements of Volatile Organic Compounds Using Proton Transfer Reaction Mass Spectrometry during the MILAGRO 2006 Campaign, *Atmos. Chem. Phys.*, 9, 467–481, 2009,  
<http://www.atmos-chem-phys.net/9/467/2009/>.

Guenther, A., Karl, T., Harley, P., Wiedinmyer, C., Palmer, P. I., and Geron, C.: Estimates of global terrestrial isoprene emissions using MEGAN (Model of Emissions of Gases and Aerosols from Nature), *Atmos. Chem. Phys.*, 6, 3181–3210, 2006,  
<http://www.atmos-chem-phys.net/6/3181/2006/>.

Guenther, A.: Corrigendum to “Estimates of global terrestrial isoprene emissions using MEGAN (Model of Emissions of Gases and Aerosols from Nature)” published in *Atmos. Chem. Phys.*, 6, 3181–3210, 2006, *Atmos. Chem. Phys.*, 7, 4327–4327, 2007,  
<http://www.atmos-chem-phys.net/7/4327/2007/>.

Hong, S.-Y., Dudhia, J., and Chen, S.-H.: A revised approach to ice microphysical processes for the parameterization of clouds and precipitation, *Mon. Weather Rev.*, 132, 103–120, 2004.

Johnson, K. S., Zuberi, B., Molina, L. T., Molina, M. J., Iedema, M. J., Cowin, J. P., Gaspar, D. J., Wang, C., and Laskin, A.: Processing of soot in an urban environment: case study from the Mexico City Metropolitan Area, *Atmos. Chem. Phys.*, 5, 3033–3043, 2005,

**Ozone response to emission changes**

J. Song et al.

Title Page

Abstract

Introduction

Conclusions

References

Tables

Figures

◀

▶

◀

▶

Back

Close

Full Screen / Esc

Printer-friendly Version

Interactive Discussion



<http://www.atmos-chem-phys.net/5/3033/2005/>.

Kain, J. S. and Fritsch, J. M.: Convective Parameterization for Mesoscale Models: The Kain-Fritsch Scheme, *The Representation of Cumulus Convection in Numerical Models*, edited by: Emanuel, K. A. and Raymond, D. J., Amer. Meteor. Soc., 246 pp., 1993.

5 Kleinman, L. I., Daum, P. H., Lee, J. H., Lee, Y.-N., Nunnermacker, L. J., Springston, S. R., Newman, L., Weinstein-Lloyd, J., and Sillman, S.: Dependence of ozone production on NO and hydrocarbons in the troposphere, *Geophys. Res. Lett.*, 24, 2299–2302, 1997.

Kleinman, L. I.: The dependence of tropospheric ozone production rate on ozone precursors, *Atmos. Environ.*, 39, 575–586, 2005.

10 Kleinman, L. I., Springston, S. R., Daum, P. H., Lee, Y.-N., Nunnermacker, L. J., Senum, G. I., Wang, J., Weinstein-Lloyd, J., Alexander, M. L., Hubbe, J., Ortega, J., Canagaratna, M. R., and Jayne, J.: The time evolution of aerosol composition over the Mexico City plateau, *Atmos. Chem. Phys.*, 8, 1559–1575, 2008, <http://www.atmos-chem-phys.net/8/1559/2008/>.

15 Lei, W., de Foy, B., Zavala, M., Volkamer, R., and Molina, L. T.: Characterizing ozone production in the Mexico City Metropolitan Area: a case study using a chemical transport model, *Atmos. Chem. Phys.*, 7, 1347–1366, 2007, <http://www.atmos-chem-phys.net/7/1347/2007/>.

20 Lei, W., Zavala, M., de Foy, B., Volkamer, R., and Molina, L. T.: Characterizing ozone production and response under different meteorological conditions in Mexico City, *Atmos. Chem. Phys.*, 8, 7571–7581, 2008, <http://www.atmos-chem-phys.net/8/7571/2008/>.

Lei, W., Zavala, M., de Foy, B., Volkamer, R., Molina, M. J., and Molina, L. T.: Impact of primary formaldehyde on air pollution in the Mexico City Metropolitan Area, *Atmos. Chem. Phys.*, 9, 2607–2618, 2009, <http://www.atmos-chem-phys.net/9/2607/2009/>.

25 Liu, Y., Bourgeois, A., Warner, T., Swerdlin, S., and Hacker, J.: Implementation of observation-nudging based FDDA into WRF for supporting ATEC test operations. 2005 WRF Users Workshop, Boulder, Colorado, June, 2005.

30 Mena-Carrasco, M., Carmichael, G. R., Campbell, J. E., Zimmerman, D., Tang, Y., Adhikary, B., D'allura, A., Molina, L. T., Zavala, M., García, A., Flocke, F., Campos, T., Weinheimer, A. J., Shetter, R., Apel, E., Montzka, D. D., Knapp, D. J., and Zheng, W.: Assessing the regional impacts of Mexico City emissions on air quality and chemistry, *Atmos. Chem. Phys.*,

**Ozone response to emission changes**

J. Song et al.

Title Page

Abstract

Introduction

Conclusions

References

Tables

Figures

◀

▶

◀

▶

Back

Close

Full Screen / Esc

Printer-friendly Version

Interactive Discussion



9, 3731–3743, 2009,

<http://www.atmos-chem-phys.net/9/3731/2009/>.

Molina, L. T. and Molina, M. J. (Eds.): Air Quality in the Mexico Megacity: An Integrated Assessment, Kluwer, Boston, 384 pp., 2002.

5 Molina, L. T., Kolb, C. E., de Foy, B., Lamb, B. K., Bruce, W. H., Jimenez, J. L., Ramos-Villegas, R., Sarmiento, J., Paramo-Figueroa, V. H., Cardenas, B., Gutierrez-Avedoy, V., and Molina, M. J.: Air quality in North America's most populous city – overview of MCMA-2003 campaign, *Atmos. Chem. Phys.*, 7, 2447–2473, 2007, <http://www.atmos-chem-phys.net/7/2447/2007/>.

10 Molina, M. J. and Molina, L. T.: Megacities and Atmospheric Pollution, *J. Air Waste Manage. Assoc.*, 54, 644–680, 2004.

Molina, L. T., Madronich, S., Gaffney, J. S., and Singh, H. B.: Overview of MILAGRO/INTEX-B campaign, in: IGAC Activities Newsletter of the International Global Atmospheric Chemistry Project, 38, 2–15, April 2008.

15 Noh, Y., Cheon, W.-G., Hong, S.-Y., and Raasch, S.: Improvement of the K-profile model for the planetary boundary layer based on large eddy simulation data, *Bound.-Lay. Meteorol.*, 107, 401–427, 2003.

Nunnermacker, L. J., Weinstein-Lloyd, J. B., Hillery, B., Giebel, B., Kleinman, L. I., Springston, S. R., Daum, P. H., Gaffney, J., Marley, N., and Huey, G.: Aircraft and ground-based measurements of hydroperoxides during the 2006 MILAGRO field campaign, *Atmos. Chem. Phys.*, 8, 7619–7636, 2008, <http://www.atmos-chem-phys.net/8/7619/2008/>.

20 Sheehy, P. M., Volkamer, R., Molina, L. T., and Molina, M. J.: Oxidative capacity of the Mexico City atmosphere – Part 2: A RO<sub>x</sub> radical cycling perspective, *Atmos. Chem. Phys. Discuss.*, 8, 5359–5412, 2008, <http://www.atmos-chem-phys-discuss.net/8/5359/2008/>.

Sillman, S.: The use of NO<sub>y</sub>, H<sub>2</sub>O<sub>2</sub>, and HNO<sub>3</sub> as indicators for ozone-NO<sub>x</sub>-hydrocarbon sensitivity in urban locations, *J. Geophys. Res.*, 100, 14175–14188, 1995.

25 Skamarock, W. C., Klemp, J. B., Dudhia, J., Gill, D. O., Barker, D. M., Wang, W., and Powers, J. G.: A description of the advanced research WRF version 2, NCAR Technical Note, NCAR/TN-468+STR, 8 pp., 2005.

30 Spencer, K. M., McCabe, D. C., Crouse, J. D., Olson, J. R., Crawford, J. H., Weinheimer, A. J., Knapp, D. J., Montzka, D. D., Cantrell, C. A., Hornbrook, R. S., Mauldin III, R. L., and

**Ozone response to emission changes**

J. Song et al.

Title Page

Abstract

Introduction

Conclusions

References

Tables

Figures

◀

▶

◀

▶

Back

Close

Full Screen / Esc

Printer-friendly Version

Interactive Discussion



Wennberg, P. O.: Inferring ozone production in an urban atmosphere using measurements of peroxyacetic acid, *Atmos. Chem. Phys.*, 9, 3697–3707, 2009, <http://www.atmos-chem-phys.net/9/3697/2009/>.

5 Springston, S. R., Kleinman, L. I., Brechtel, F., Lee, Y.-N., and Nunnermacker, L. J.: Chemical evolution of an isolated power plant plume during the TexAQS 2000 study, *Atmos. Environ.*, 39, 3431–3443, 2005.

Stephens, S., Madronich, S., Wu, F., Olson, J. B., Ramos, R., Retama, A., and Muñoz, R.: Weekly patterns of México City's surface concentrations of CO, NO<sub>x</sub>, PM<sub>10</sub> and O<sub>3</sub> during 1986–2007, *Atmos. Chem. Phys.*, 8, 5313–5325, 2008, <http://www.atmos-chem-phys.net/8/5313/2008/>.

10 Stremme, W., Ortega, I., and Grutter, M.: Using ground-based solar and lunar infrared spectroscopy to study the diurnal trend of carbon monoxide in the Mexico City boundary layer, *Atmos. Chem. Phys.*, 9, 8061–8078, 2009, <http://www.atmos-chem-phys.net/9/8061/2009/>.

15 Tie, X., Madronich, S., Li, G., Ying, Z., Zhang, R., Garcia, A., Lee-Taylor, J., and Liu, Y.: Characterization of chemical oxidants in Mexico City: A regional chemical dynamical model (WRFCHEM) study, *Atmos. Environ.*, 41, 1989–2008, 2007.

Tonnesen, G. S. and Dennis, R. L.: Analysis of radical propagation efficiency to assess ozone sensitivity to hydrocarbons and NO<sub>x</sub>, 1. Local indicators of instantaneous odd oxygen production sensitivity, *J. Geophys. Res.*, 105(D7), 9213–9225, 2000.

20 Torres-Jardon, R.: Comparative Assessment of the Sensitivity of Ozone to Nitrogen Oxides and Volatile Organic Compounds in Two Dissimilar Metropolitan Areas of North America: Cincinnati, OH (USA) and Mexico City, DF (Mexico), Ph. D. Thesis, University of Cincinnati, 2004.

25 Velasco, E., Pressley, S., Grivicke, R., Allwine, E., Coons, T., Foster, W., Jobson, B. T., Westberg, H., Ramos, R., Hernández, F., Molina, L. T., and Lamb, B.: Eddy covariance flux measurements of pollutant gases in urban Mexico City, *Atmos. Chem. Phys.*, 9, 7325–7342, 2009, <http://www.atmos-chem-phys.net/9/7325/2009/>.

30 Volkamer, R., Sheehy, P. M., Molina, L. T., and Molina, M. J.: Oxidative capacity of the Mexico City atmosphere Part 1: A radical source perspective, *Atmos. Chem. Phys. Discuss.*, 7, 5365–5412, 2007, <http://www.atmos-chem-phys-discuss.net/7/5365/2007/>.

**Ozone response to emission changes**

J. Song et al.

Title Page

Abstract

Introduction

Conclusions

References

Tables

Figures

◀

▶

◀

▶

Back

Close

Full Screen / Esc

Printer-friendly Version

Interactive Discussion



**Ozone response to emission changes**

J. Song et al.

- West, J. J., Zavala, M. A., Molina, L. T., Molina, M. J., San Martini, F., McRae, G. J., Sosa-Iglesias, G., and Arriaga-Colina, J. L.: Modeling ozone photochemistry and evaluation of hydrocarbon emissions in the Mexico City metropolitan area, *J. Geophys. Res.*, 109, D19312, doi:10.1029/2004JD004614, 2004.
- 5 Wood, E. C., Herndon, S. C., Onasch, T. B., Kroll, J. H., Canagaratna, M. R., Kolb, C. E., Worsnop, D. R., Neuman, J. A., Seila, R., Zavala, M., and Knighton, W. B.: A case study of ozone production, nitrogen oxides, and the radical budget in Mexico City, *Atmos. Chem. Phys.*, 9, 2499–2516, 2009, <http://www.atmos-chem-phys.net/9/2499/2009/>.
- 10 Zavala, M., Lei, W., Molina, M. J., and Molina, L. T.: Modeled and observed ozone sensitivity to mobile-source emissions in Mexico City, *Atmos. Chem. Phys.*, 9, 39–55, 2009, <http://www.atmos-chem-phys.net/9/39/2009/>.
- Zavala, M., Herndon, S. C., Wood, E. C., Onasch, T. B., Knighton, W. B., Marr, L. C., Kolb, C. E., and Molina, L. T.: Evaluation of mobile emissions contributions to Mexico City's emissions inventory using on-road and cross-road emission measurements and ambient data, *Atmos. Chem. Phys.*, 9, 6305–6317, 2009, <http://www.atmos-chem-phys.net/9/6305/2009/>.
- 15 Zhao, J. and Zhang, R. Y.: Proton transfer reaction rate constants between hydroxium ion ( $\text{H}_3\text{O}^+$ ) and volatile organic compounds, *Atmos. Environ.*, 38, 2177–2185, doi:10.1016/j.atmosenv.2004.01.019, 2004.
- 20

[Title Page](#)[Abstract](#)[Introduction](#)[Conclusions](#)[References](#)[Tables](#)[Figures](#)[I◀](#)[▶I](#)[◀](#)[▶](#)[Back](#)[Close](#)[Full Screen / Esc](#)[Printer-friendly Version](#)[Interactive Discussion](#)

## Ozone response to emission changes

J. Song et al.

**Table 1.** VOC measurements during the MILAGRO campaign that were used in this study.

Site/Platform	Analytical method	VOCs used in the analysis	Institution
CENICA	GC-FID	ethane, propane, acetylene, toluene, benzene, and xylene	INE, MX
SIMAT T0	EC-FOS	Propene-equivalent olefins	WSU
	GC and GC/MS	ethane, ethene, propane, acetylene, toluene, benzene, xylene, i-butene, 1-pentene, 1,3-butadiene, t-2-butene, c-2-butene, t-2-pentene, and c-2-pentene	UC Irvine
	PTRMS DOAS	acetaldehyde, toluene, and benzene benzene, toluene, o-xylene, m-xylene, p-xylene, phenol, cresol, formaldehyde, and benzaldehyde	Texas A&M U. MIT/ Univ. Heidelberg
	TDLAS and PTRMS	formaldehyde, acetaldehyde, ethene, toluene, and benzene	ARI
G-1 aircraft	GC/PTRMS	ethene, ethane, propane, benzene, toluene, xylenes, trimethyl-benzene; CO and O <sub>3</sub> (non-VOCs)	BNL/PNNL

Title Page

Abstract

Introduction

Conclusions

References

Tables

Figures

I◀

▶I

◀

▶

Back

Close

Full Screen / Esc

Printer-friendly Version

Interactive Discussion



## Ozone response to emission changes

J. Song et al.

**Table 2.** Comparison between total weekday emissions by pollutant type and source category in the MCMA from the 2006 official emission inventory and the adjusted emissions used in this study. Units are in tons day<sup>-1</sup>. Numbers in parenthesis indicate the domain-wide emissions.

Source category	2006 official EI			Adjusted EI		
	CO	NO <sub>x</sub>	VOCs	CO	NO <sub>x</sub>	VOCs
Area	5460	470	1160	5460	470	1520
Point	20	60	330	20	60	300
Biogenic	0	0	80	10	0	110–220
<b>Total</b>	<b>5480</b>	<b>540</b>	<b>1570</b>	<b>5490</b> (12 030–12 050)	<b>540 (850)</b>	<b>1920–2040</b> (6440–7280)

Title Page

Abstract

Introduction

Conclusions

References

Tables

Figures

I◀

▶I

◀

▶

Back

Close

Full Screen / Esc

Printer-friendly Version

Interactive Discussion



## Ozone response to emission changes

J. Song et al.

**Table 3.** Percentage changes of episode averaged peak ozone concentrations due to emission reductions under different meteorological conditions.

Episode	Base case O <sub>3</sub> (ppb)	50% VOC (%)	50% NO <sub>x</sub> (%)	50% All (%)
O <sub>3</sub> -SV	66.9	−24.5	36.3	−8.1
O <sub>3</sub> -N1	93.5	−32.8	18.4	−14.2
O <sub>3</sub> -S	84.3	−34.2	37.7	−7.5
O <sub>3</sub> -N2	70.9	−16.6	9.2	−6.9
O <sub>3</sub> -CnvS	80.4	−26.9	14.7	−9.3
O <sub>3</sub> -CnvN	78.0	−23.7	23.6	−6.8

[Title Page](#)[Abstract](#)[Introduction](#)[Conclusions](#)[References](#)[Tables](#)[Figures](#)[I◀](#)[▶I](#)[◀](#)[▶](#)[Back](#)[Close](#)[Full Screen / Esc](#)[Printer-friendly Version](#)[Interactive Discussion](#)

Ozone response to  
emission changes

J. Song et al.

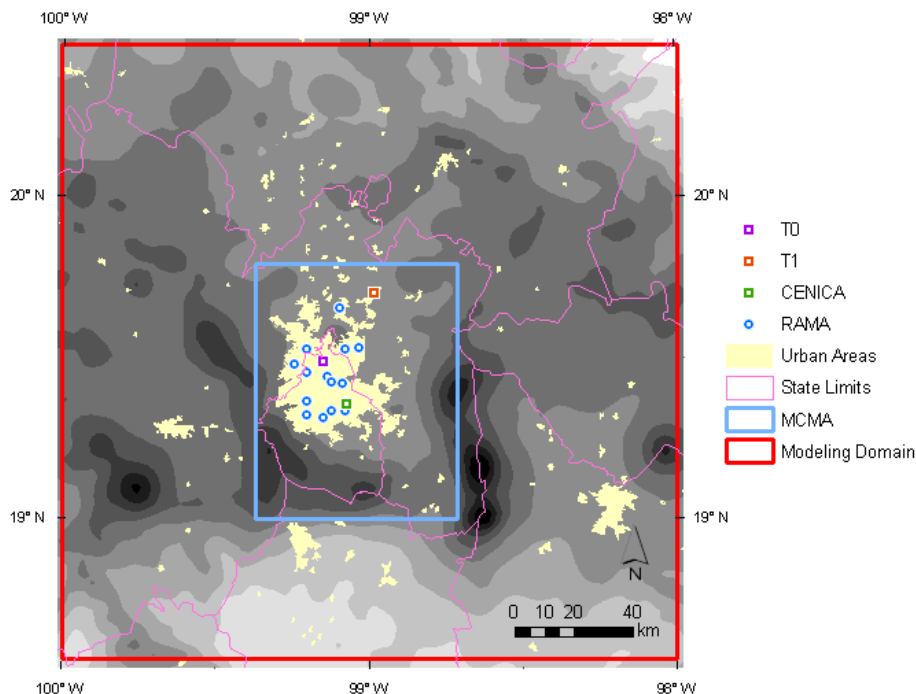


**Fig. 1.** Air quality modeling domain (3 km by 3 km; the outer red square) with RAMA monitoring sites (blue), CENICA site (green), T0 supersite (purple), and T1 supersite (orange) from the MCMA-2006 field campaign. Light blue domain indicates the area covered by 2006 official emission inventory for MCMA, 2006 EI. Light yellow shading denotes urban areas. Topography contour intervals are 400 m, and the pink contour represents the political state limits.

[Title Page](#)[Abstract](#)[Introduction](#)[Conclusions](#)[References](#)[Tables](#)[Figures](#)[◀](#)[▶](#)[◀](#)[▶](#)[Back](#)[Close](#)[Full Screen / Esc](#)[Printer-friendly Version](#)[Interactive Discussion](#)

## Ozone response to emission changes

J. Song et al.

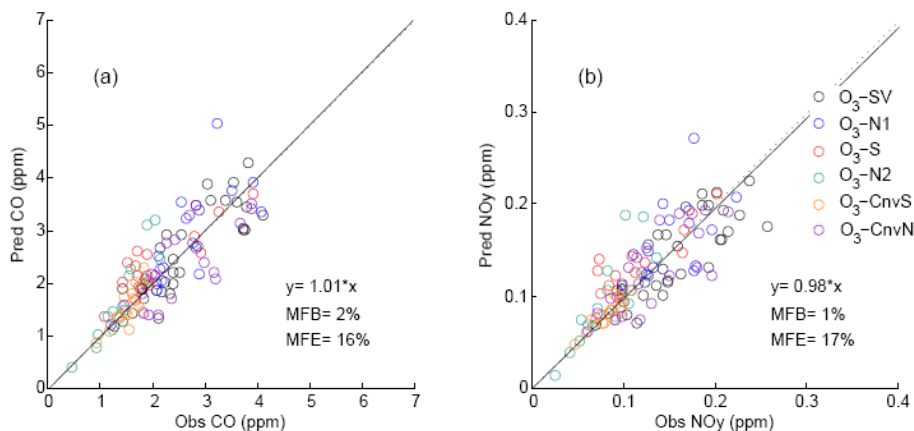


**Fig. 2.** Scatter plot of simulated and observed concentrations of **(a)** CO and **(b)** NO<sub>y</sub> over 15 RAMA monitoring sites during all episodes. Scatter plots only show datasets during 07:00–11:00LT for CO and NO<sub>y</sub>. Performance statistics are also shown. The dashed lines indicate a perfect positive correlation, and each color indicates a different meteorological episode.

[Title Page](#)[Abstract](#)[Introduction](#)[Conclusions](#)[References](#)[Tables](#)[Figures](#)[◀](#)[▶](#)[◀](#)[▶](#)[Back](#)[Close](#)[Full Screen / Esc](#)[Printer-friendly Version](#)[Interactive Discussion](#)

## Ozone response to emission changes

J. Song et al.

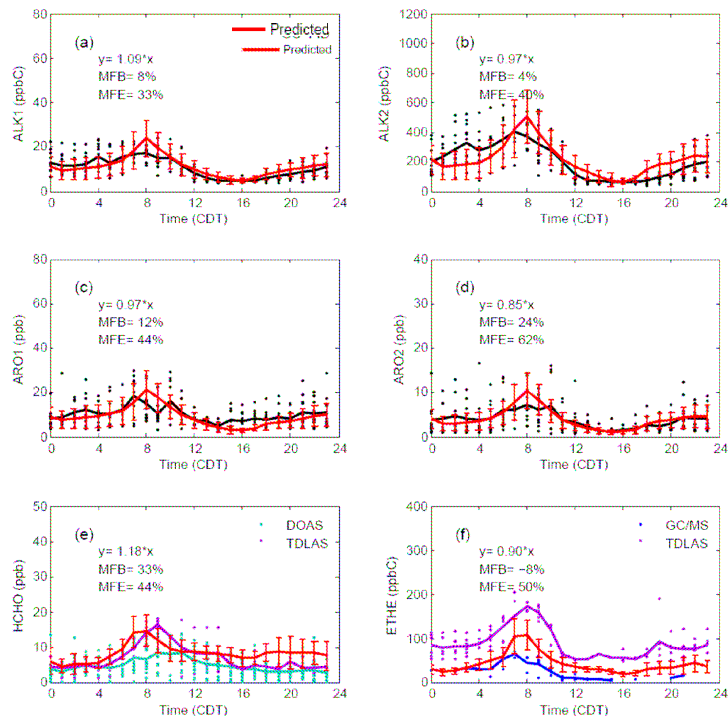


**Fig. 3.** Comparisons of simulated and observed VOC concentrations after the emissions were adjusted. **(a)** ALK1, **(b)** ALK2, **(c)** ARO1, **(d)** ARO2 at CENICA, and **(e)** HCHO, **(f)** ETHE at T0. Measurements within 5 and 95 percentiles are included. Each colored dot indicates individual VOC measurement, and the solid line with corresponding color indicates the average of those measurements. Different color indicates different measurement techniques: GC-FID data in black, DOAS data in light green, TDLAS data in purple, GC and GC/MS data in blue. Hourly averaged simulated VOC concentrations with  $\pm 1$  standard deviation (averaged over the time concurrent to the VOC observations at CENICA and T0 in March 2006) are shown in red. Also shown are the agreement statistics ( $y$ =simulations,  $x$ =observations) during 06:00–11:00 a.m.

Title Page

Abstract

Introduction

Conclusions

References

Tables

Figures

◀

▶

◀

▶

Back

Close

Full Screen / Esc

Printer-friendly Version

Interactive Discussion



## Ozone response to emission changes

J. Song et al.

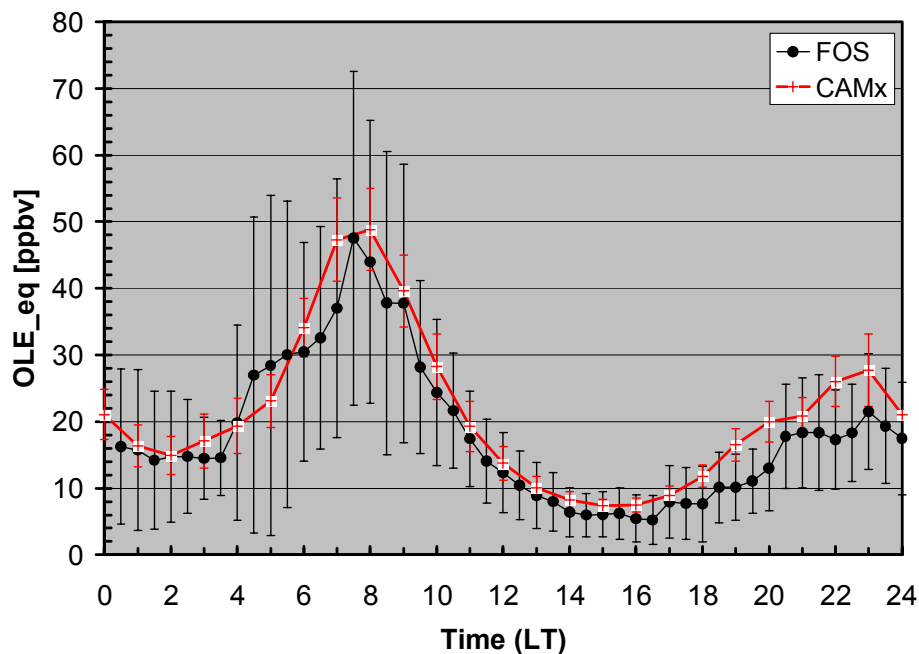


**Fig. 4.** Comparison of simulated (in red) and measured (in black) average diurnal variations of propene-equivalent olefin concentrations at SIMAT. Error bars represent  $\pm 1$  standard deviations, indicating the inter-diurnal variability. Data were averaged over 10–28 March 2006.

[Title Page](#)[Abstract](#)[Introduction](#)[Conclusions](#)[References](#)[Tables](#)[Figures](#)[◀](#)[▶](#)[◀](#)[▶](#)[Back](#)[Close](#)[Full Screen / Esc](#)[Printer-friendly Version](#)[Interactive Discussion](#)

## Ozone response to emission changes

J. Song et al.

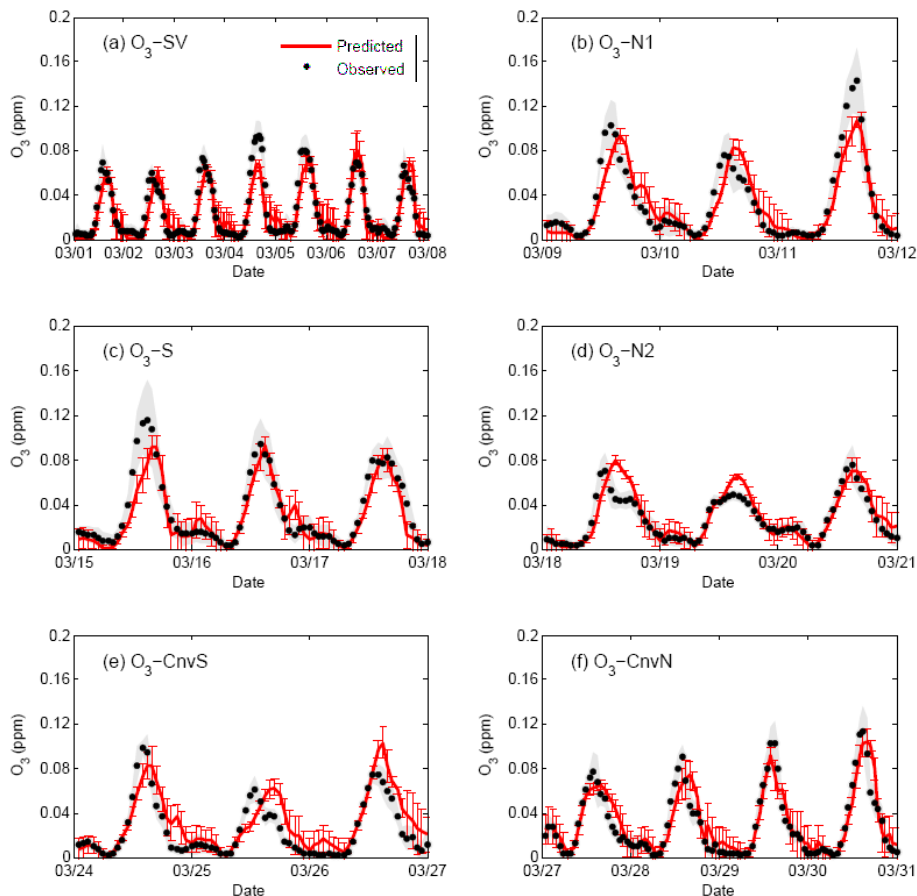


**Fig. 5.** Comparison of hourly simulated concentrations of  $O_3$  with the observations averaged over 15 RAMA monitoring sites during (a)  $O_3$ -SV, (b)  $O_3$ -N1, (c)  $O_3$ -S, (d)  $O_3$ -N2, (e)  $O_3$ -CnvS, and (f)  $O_3$ -CnvN episode. Shaded area and error bars indicate  $\pm 1$  standard deviation of the observation and simulation, respectively.

[Title Page](#)[Abstract](#)[Introduction](#)[Conclusions](#)[References](#)[Tables](#)[Figures](#)[◀](#)[▶](#)[◀](#)[▶](#)[Back](#)[Close](#)[Full Screen / Esc](#)[Printer-friendly Version](#)[Interactive Discussion](#)

Ozone response to  
emission changes

J. Song et al.

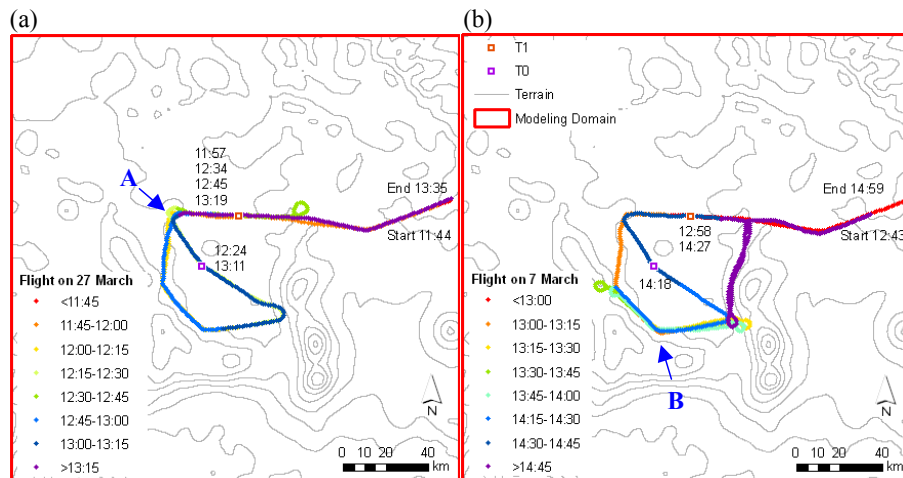


**Fig. 6.** Flight track of the G-1 aircraft on **(a)** 27 and **(b)** 7 March with starting, ending, and sampling time stamps at each supersite from MCMA-2006 field campaign are shown; T0 (purple) and T1 (orange). Rainbow colors correspond to the measurement time. Topography contour intervals are 400 m. Letter A and B denote the location where flights passed multiple times.

Title Page

Abstract

Introduction

Conclusions

References

Tables

Figures

◀

▶

◀

▶

Back

Close

Full Screen / Esc

Printer-friendly Version

Interactive Discussion



## Ozone response to emission changes

J. Song et al.

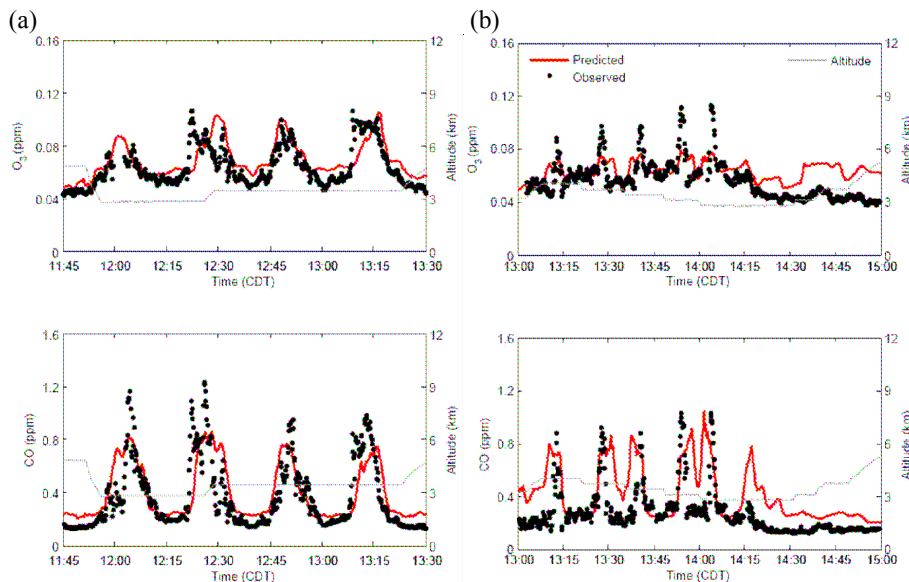


**Fig. 7.** Time series for ozone and CO along the G-1 flight track on **(a)** 27 and **(b)** 7 March. Each measurement was taken at a 10-s interval, and simulations were temporally and spatially interpolated simulations to correspond each measurement. Gray line indicates the G-1 flight altitude.

[Title Page](#)[Abstract](#)[Introduction](#)[Conclusions](#)[References](#)[Tables](#)[Figures](#)[◀](#)[▶](#)[◀](#)[▶](#)[Back](#)[Close](#)[Full Screen / Esc](#)[Printer-friendly Version](#)[Interactive Discussion](#)

## Ozone response to emission changes

J. Song et al.

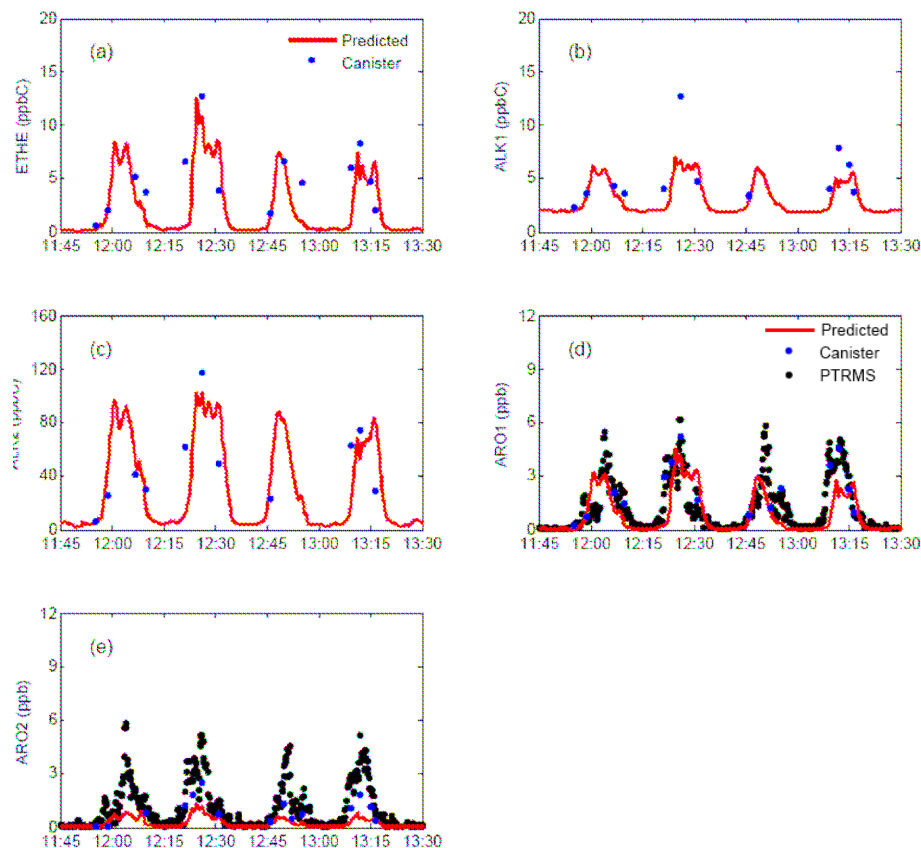


**Fig. 8.** Time series for VOCs on 27 March are shown. Canister measurements were collected within 1–2 min (blue dots), and real-time VOCs analyzed by PTRMS were taken at 10-s intervals (black dots). Simulations were temporally and spatially interpolated to correspond to each measurement.

[Title Page](#)[Abstract](#)[Introduction](#)[Conclusions](#)[References](#)[Tables](#)[Figures](#)[◀](#)[▶](#)[◀](#)[▶](#)[Back](#)[Close](#)[Full Screen / Esc](#)[Printer-friendly Version](#)[Interactive Discussion](#)

## Ozone response to emission changes

J. Song et al.

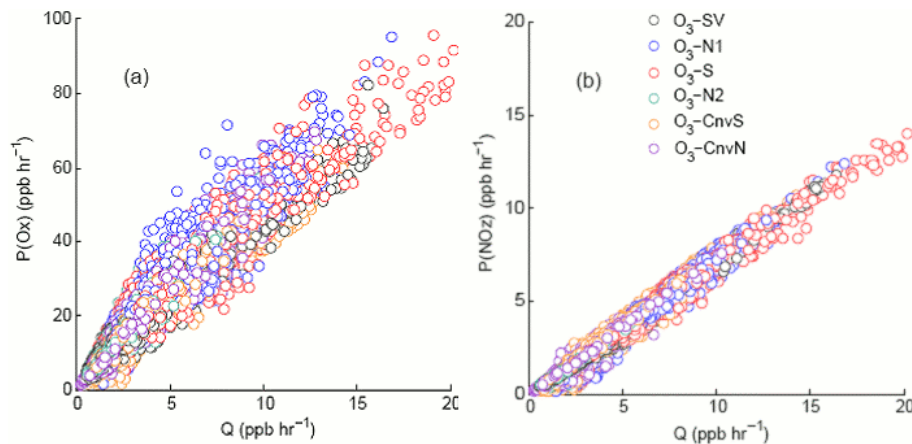


**Fig. 9.** Indicators examining the VOC- or NO<sub>x</sub>-limited conditions for urban area during 12:00–17:00 LT; Relationships between primary radical production rates and **(a)** O<sub>x</sub> formation rate and **(b)** NO<sub>x</sub> oxidation rate.

[Title Page](#)[Abstract](#)[Introduction](#)[Conclusions](#)[References](#)[Tables](#)[Figures](#)[I◀](#)[▶I](#)[◀](#)[▶](#)[Back](#)[Close](#)[Full Screen / Esc](#)[Printer-friendly Version](#)[Interactive Discussion](#)

## Ozone response to emission changes

J. Song et al.

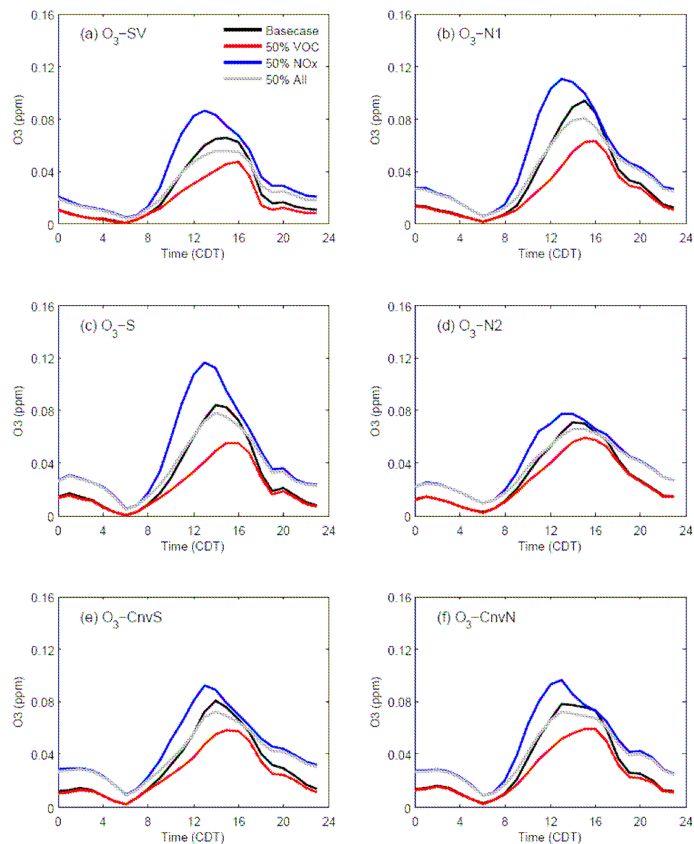


**Fig. 10.** Time series showing the sensitivity of ozone production to ozone precursors under different meteorological conditions, compared to the base case. Data were averaged over 15 RAMA monitoring stations and over each period. Black line indicates the base case, red indicates the ozone concentrations with 50% reductions in VOC emissions, blue indicates those with 50% reductions in NO<sub>x</sub> emissions, and gray indicates those with 50% reductions in both VOC and NO<sub>x</sub> emissions.

[Title Page](#)[Abstract](#)[Introduction](#)[Conclusions](#)[References](#)[Tables](#)[Figures](#)[◀](#)[▶](#)[◀](#)[▶](#)[Back](#)[Close](#)[Full Screen / Esc](#)[Printer-friendly Version](#)[Interactive Discussion](#)

## Ozone response to emission changes

J. Song et al.

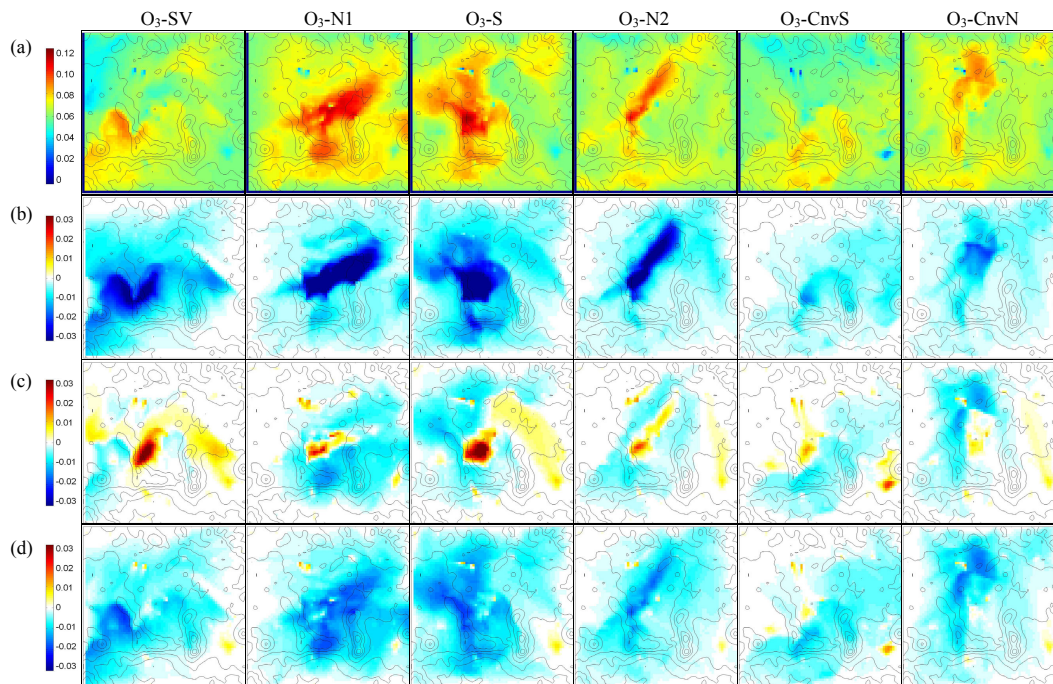


**Fig. 11.** Spatial distribution of peak ozone changes due to the changes in emissions under different meteorological conditions. **(a)** Peak ozone concentration in the base case, **(b)** ozone change with 50% VOC, **(c)** ozone change with 50%  $\text{NO}_x$ , and **(d)** ozone change with 50% VOC and  $\text{NO}_x$ . Snapshots were taken at peak ozone hours, units are in ppm.

[Title Page](#)[Abstract](#)[Introduction](#)[Conclusions](#)[References](#)[Tables](#)[Figures](#)[I◀](#)[▶I](#)[◀](#)[▶](#)[Back](#)[Close](#)[Full Screen / Esc](#)[Printer-friendly Version](#)[Interactive Discussion](#)

## Ozone response to emission changes

J. Song et al.

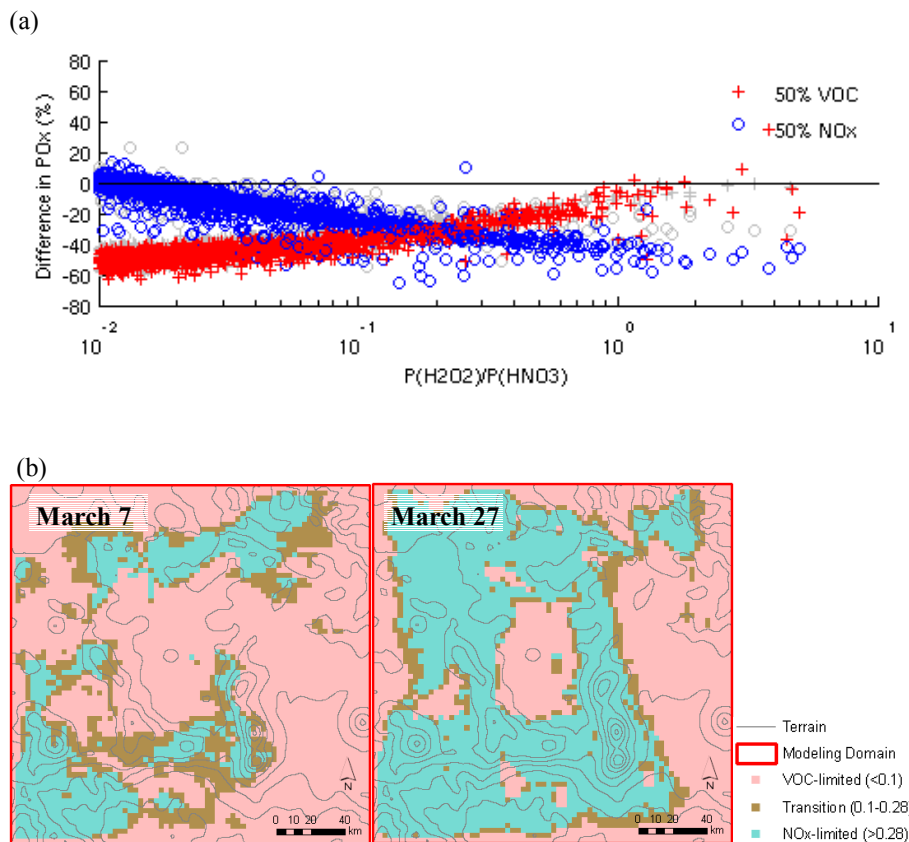


**Fig. 12.** (a) The percentage change in  $O_x$  formation rate as a function of the indicator, ratio of  $H_2O_2$  production rate to  $HNO_3$  production rate at 12:00–17:00 LT during the episodes (week-ends are shown in gray) within the urban area, (b) spatial distribution of the ratio at 14:00 LT on 7 and 27 March. Topography contour intervals are 400 m.

Title Page

Abstract

Introduction

Conclusions

References

Tables

Figures

◀

▶

◀

▶

Back

Close

Full Screen / Esc

Printer-friendly Version

Interactive Discussion



## Ozone response to emission changes

J. Song et al.

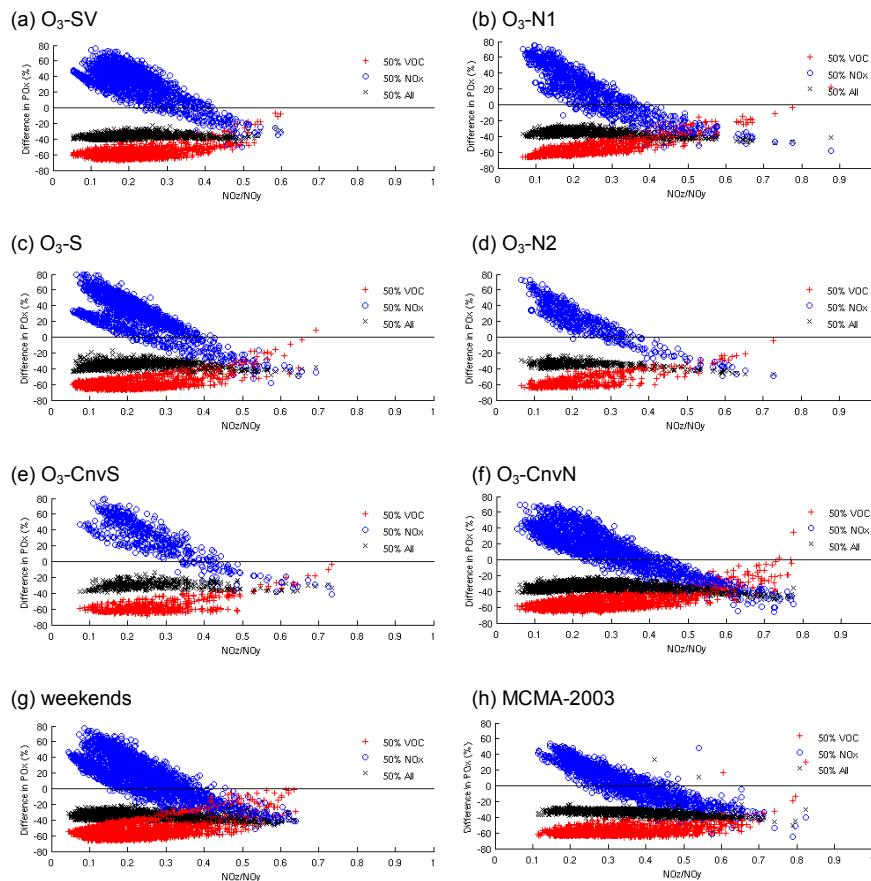


**Fig. 13.** Percentage change of  $P(O_x)$  as a function of chemical aging in the urban area at 12:00–17:00 LT during (a–g) MCMA-2006 and (h) MCMA-2003. (a–g) were sampled on weekdays during different meteorological episodes, (g) was sampled on weekends, and (h) was sampled during a  $O_3$ -South episode.

Title Page

Abstract

Introduction

Conclusions

References

Tables

Figures

◀

▶

◀

▶

Back

Close

Full Screen / Esc

Printer-friendly Version

Interactive Discussion



## Ozone response to emission changes

J. Song et al.

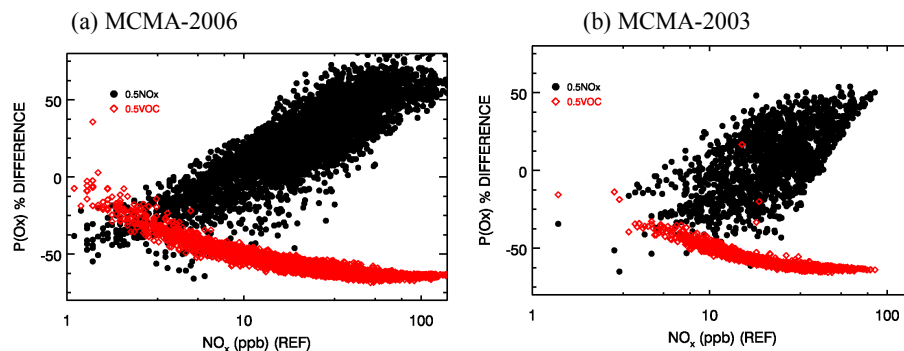


**Fig. 14.** Simulated percentage change of  $P(O_x)$  as a function of base case  $NO_x$  in the urban area at 12:00–17:00 LT during (a) MCMA-2006 and (b) MCMA-2003. Datapoints in (a) include weekdays only throughout the whole episode.

[Title Page](#)[Abstract](#)[Introduction](#)[Conclusions](#)[References](#)[Tables](#)[Figures](#)[I◀](#)[▶I](#)[◀](#)[▶](#)[Back](#)[Close](#)[Full Screen / Esc](#)[Printer-friendly Version](#)[Interactive Discussion](#)